Review

Metal Oxide-Related Dendritic Structures: Self-Assembly and Applications for Sensor, Catalysis, Energy Conversion and Beyond

Ruohong Sui [1,*] **, Paul A. Charpentier** [2] **and Robert A. Marriott** [1,*]

1   Department of Chemistry, University of Calgary, Calgary, AB T2L 2K8, Canada
2   Department of Chemical and Biochemical Engineering, Western University, London, ON N6A 5B9, Canada; pcharpen@uwo.ca
*   Correspondence: rsui@ucalgary.ca (R.S.); rmarriot@ucalgary.ca (R.A.M.)

Abstract: In the past two decades, we have learned a great deal about self-assembly of dendritic metal oxide structures, partially inspired by the nanostructures mimicking the aesthetic hierarchical structures of ferns and corals. The self-assembly process involves either anisotropic polycondensation or molecular recognition mechanisms. The major driving force for research in this field is due to the wide variety of applications in addition to the unique structures and properties of these dendritic nanostructures. Our purpose of this minireview is twofold: (1) to showcase what we have learned so far about how the self-assembly process occurs; and (2) to encourage people to use this type of material for drug delivery, renewable energy conversion and storage, biomaterials, and electronic noses.

Keywords: dendritic metal oxide; self-assembly; sol-gel; hydrothermal; molecular recognition

1. Introduction

A dendritic structure exhibits a tree-like shape containing stems and branches. It can be a macromolecule, supramolecule, or nanostructure. Despite appearing otherwise in literature, herein "dendrites" mean the dendritic structures of crystals or metals (such as gold, silver, and copper) [1,2], while dendrimers refer to highly branched macromolecules or supramolecules.

Since the discovery of dendrimers in 1978 [3], the number of reports regarding the syntheses of these types of materials has grown exponentially. Most dendrimers reported in literature are organic oligomers, macromolecules, and supramolecules, which may contain metal- or silicon-ligand moieties [4–8]. Specifically, the dendritic transition-metal complexes and metallodendrimers were well discussed by Astruc and Chardac [9]. Figure 1 shows the dendrimers of polyethylene and polyglycerol, which have been graphed on ceramic membranes using -OSiO- bond as a link. The resulting composite materials were found to efficiently remove aromatic hydrocarbons and trihalogen methanes from water [10].

Not so long ago, dendritic nanostructures of metal oxides or organic-inorganic hybrids emerged from the field of material science. These dendritic structures are composed of organized 1D or 2D inorganic particulates [11], and the latter is made of 1D or 2D macromolecules/supramolecules (Scheme 1). Noticeably, most of these materials are prepared through self-assembly via a sol-gel or hydrothermal route, which often involves supramolecular organization via molecular recognition between the specially designed species (e.g., between the oligomers and surfactants) [12]. Chemical vapor deposition and electrodeposition are also well-established approaches for making sophisticated nanostructures [13,14], but the sol-gel and hydrothermal methods are more scalable for commercialization. Due to their special hierarchical nanostructures, dendritic metal oxides exhibit open macropores (>50 nm) and the large mesopores (2–50 nm). This makes most of their surface area available for large molecules or causes a situation where mass transfer is the

bottleneck of a process. In a water splitting process, for instance, the produced hydrogen bubbles can be trapped within the pores of electrodes, which makes it difficult for water molecules to access the active sites of the catalyst [15]. This problem can be solved by using the electrode with a dendritic nanostructure.
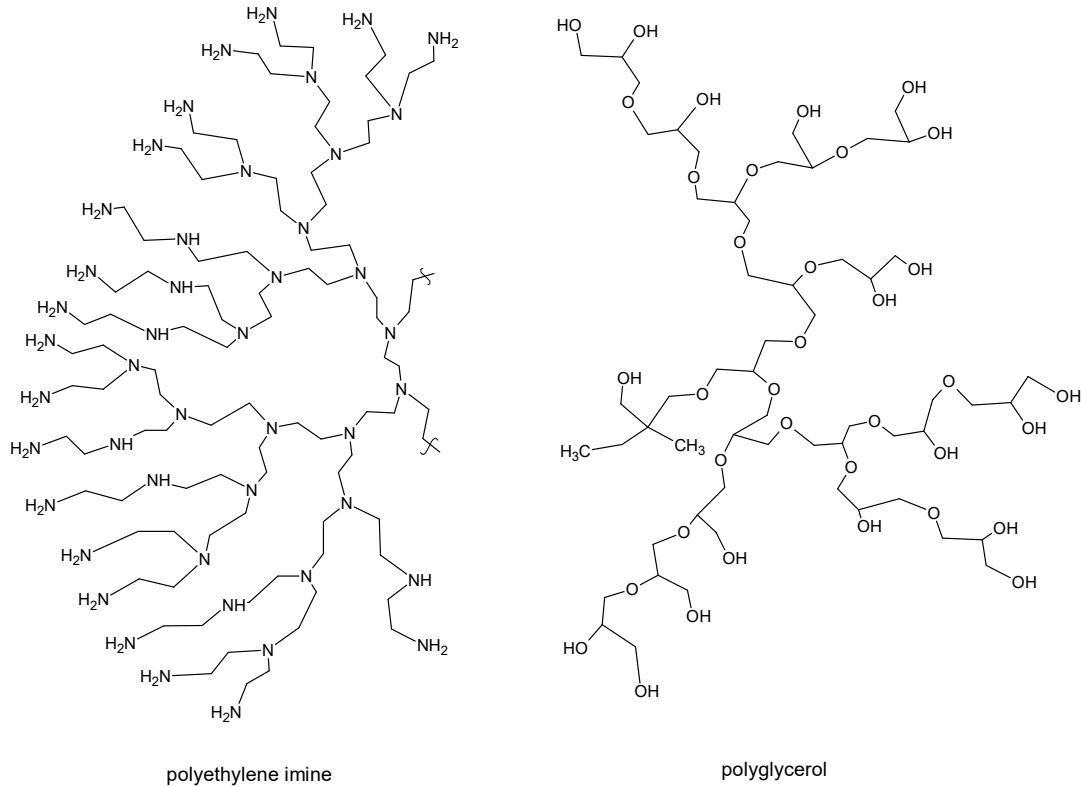

polyethylene imine   polyglycerol

Figure 1. Examples of dendritic oligomers that are used to modify ceramic filters to remove organic contaminants from water [10].

1D macro/supramolecules　　　　1D particulate　　　　dendritic metal oxide

2D macro/supramolecules　　　　2D particulate　　　　dendritic metal oxide
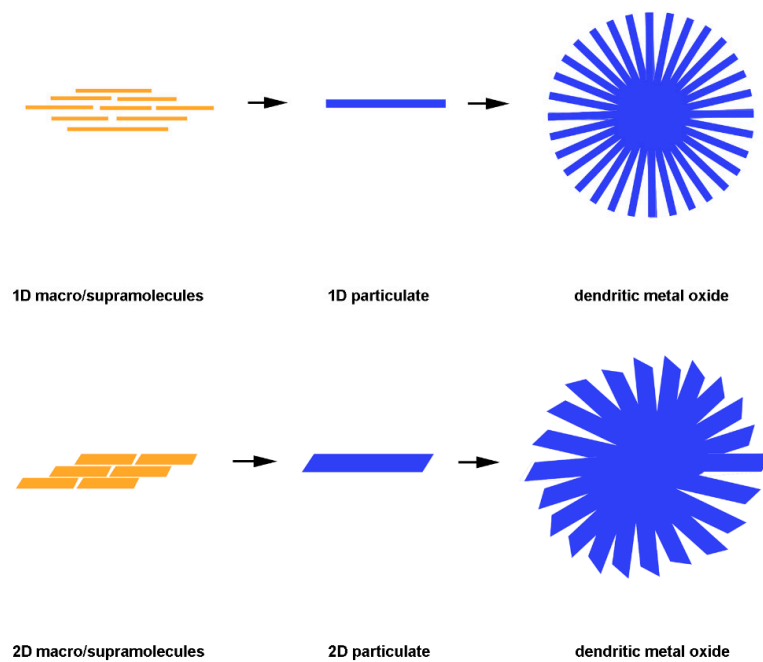
Scheme 1. Dendritic metal oxides are organized 1D or 2D particulates in certain patterns. The particulates are composed of 1D or 2D macromolecules/supramolecules.

Dendritic metal oxides are potentially useful in the fields of medicine [16–18], biomaterials [19], heterogeneous catalysis [20], protective coatings [21–24], molecular machines [25], energy conversion and storage [26], sensing electronics [27–29], and low-voltage transistors [30–33]. Recently, another type of dendritic structure has caught people's attention: dendritic meso-pores. These radially aligned channels are generated within spherical particles [34,35]. These dendritic pores are different from the parallel mesopore channels within silicate MCM-41, a milestone work performed by Mobil Oil Cooperation [36].

The purpose of this paper is to review, from the synthesis and application perspectives, metal oxide-based dendritic nanostructures.

2. Synthesis of Dendritic Metal Oxides

2.1. Sol-Gel Method

The first documented sol-gel synthesis appeared in 1939, when Geffcken and Berger described their novel oxide coating technique [37]. Because sol-gel processing is easy for scale-up and process control, this technique has been commercialized for coating thin films and making ceramic fibers and/or aerogels [38]. During the past few decades, sol-gel technologies have made significant progress towards developing mesoporous materials, nanoparticles (0D), one-dimensional (1D), two-dimensional (2D), and three-dimensional (3D) metal oxides [39–42]. Conventional sol-gel reactions involve hydrolysis and poly-condensation of metal salts or alkoxides in a solvent medium, such as water, an organic solvent, ionic liquid, or a supercritical fluid. For making a well-defined nanostructure, one needs to control the rates of reaction between a metal precursor (such as titanium isopropoxide) and water. This can be achieved by addition of carboxylic acids, alcohols, or surfactants [43]. It was found that addition of propylene oxide in the starting materials facilitates gel formation [44,45]. The bench-top equipment for sol-gel synthesis can be as simple as a round-bottom flask sitting on a hot plate and stirrer. Alternatively, one can use a stainless-steel view cell reactor that can be heated and pressurized to 35 megapascals [41]. By taking advantage of better mass and heat transfer in supercritical carbon dioxide (scCO$_2$), self-assembly of titanium-oxo-alkoxyl-acetate complexes (Ti$_6$O$_6$(OAc)$_6$(O^{i}Pr)$_6$) results in dendritic nanostructures of Ti$_6$O$_9$(OAc)$_6$. The later can be calcined in air to form titania (TiO$_2$) (Figure 2a,b) [46]. When isopropanol is used, interestingly, dendritic TiO$_2$ can be prepared which is composed of 2D structures (Figure 2c,d) [47]. Due to a high surface area and large pore size, this type of material shows advantages over traditional catalysts for industrial applications [48–50]. The sol-gel self-assembly will be discussed further in the following section.

A spin coating of sol-gel fluid can be used for preparing dendritic zinc stannate in a thin film, which is a sensor material for detecting certain chemicals in liquified petroleum, such as ethanol, formaldehyde, and hydrogen sulfide [51]. The hierarchical structures exhibit an open surface that facilitates diffusion of target molecules in a liquid phase. In addition, the dendritic structures are more anti-fouling than microporous counterparts, even though the latter often exhibit a higher surface area. Polyethylene glycol may play multiple roles, such as in preventing precipitation of the metal precursors in sol-gel process, as well as in avoiding shrinkage and cracking upon drying [52].

By using cetyltrimethylammonium bromide (CTAB) as a surfactant, hydrolysis and polycondensation of tetraethyl orthosilicate (TEOS) can produce a dendritic microstructure of silica with encapsulated phenolphthalein, which can form an opto-chemical sensor device [53]. Alternatively, a thin film of dendritic polymer/SiO$_2$ can be prepared by polycondensation of mixed silicon alkoxide: Si(OR)$_4$, R'Si(OR)$_3$, and R'HSi(OR)$_2$, where R and R' stand for CH$_3$ and C$_2$H$_5$ alkyl groups, respectively [54]. Because the R'-Si bond is inert and hydrolysis and condensation only occur on the -OR ligands, anisotropic condensation can be expected from sol-gel reactions of R'Si(OR)$_3$ and R'HSi(OR)$_2$. Hence, it is not surprising to observe dendritic structures from these precursors. By using tetraethyl orthosilicate and metal (Fe, Ni, and Co) chlorides as precursors, a dendritic magnetic

nanocomposite structure can be obtained via a sol-gel route, followed by annealing up to 1373 K [55]. The resulting materials can be used for medical or information storage systems.
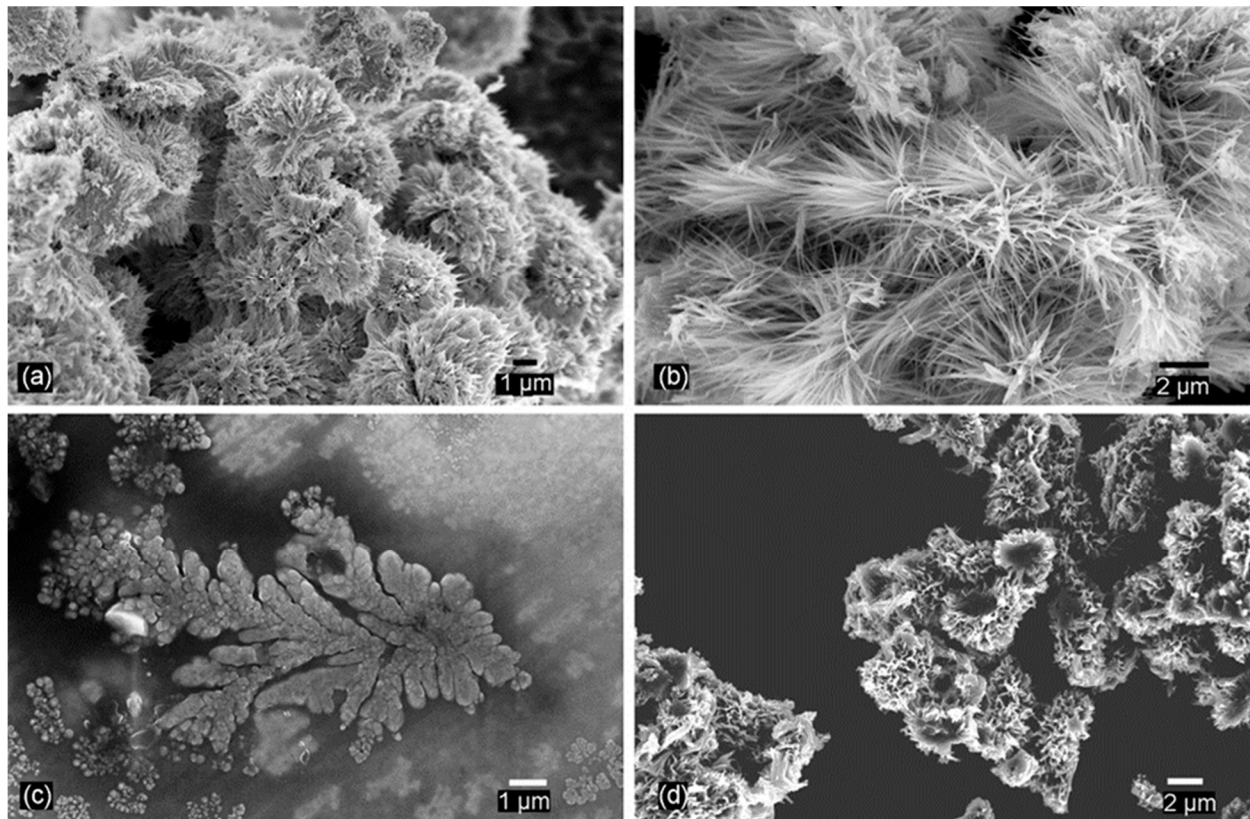

Figure 2. SEM images of TiO$_2$ dendritic nanostructures prepared via sol-gel reactions of titanium isopropoxide with acetic acid in scCO$_2$ (**a,b**) and isopropanol (**c,d**).

Self-assembly also is a powerful tool for synthesizing hydrogels with an internal dendritic structure. For example, Ga^{3+} anionic metal-organic cubes were linked together by using ammonium or amine-based ions as a binder to form dendritic supramolecules [56]. This type of material is useful for gel-chromatographic separation of dyes, and it can also be an intermediate for hybrid metal oxides.

In Table 1, both the advantages and disadvantages of sol-gel method are summarized, which can be compared with other synthesis methods in terms of their advantage, scalability, and production cost for a commercial scale production.

Table 1. Comparison of synthesis methods for making dendritic metal oxides.

Methods	Advantages	Disadvantages	Scalability	Cost
Sol-gel	mild synthesis conditions, low reaction temperature	long reaction time, organic solvents	high	low
Hydro-/solvothermal	short reaction time	anti-corrosive and pressure vessels, organic solvents, and surfactants	high	high
Electrochemical	involving less chemicals	energy intensive	relatively low	high
Supramolecular self-assembly	mild synthesis conditions, low reaction temperature	organic solvents and surfactants	high	low

2.2. Hydrothermal and Solvothermal Methods

The discovery of this method can be dated back to the middle of 19th century, when K.F.E. Schafthaul synthesized quartz crystals within supercritical water [57]. By taking advantage of a high temperature, high density, and high viscosity of water or other solvents above ambient pressure, one can grow both microscopic and macroscopic crystals. In the past two decades hydrothermal/solvothermal methods have been widely used for preparing metal oxides with different sizes and morphologies. The operation temperature can be diversified from as high as 673 K to as low as 353 K [58]. In the early days, Bunsen used thick-walled glass barometer tubing for his synthesis of $BaCO_3$ and $SrCO_3$ crystals at 473 K and 1.5 megapascal [59]. Nowadays, a Teflon-lined stainless-steel autoclave is widely available for bench-scale synthesis. The starting materials can be varied from metal alkoxide to salts and even a metal oxide itself [60].

Hydrothermal or solvothermal techniques are also useful for synthesizing dendritic TiO_2, as reviewed by Wu and coworkers [61]. It was found that the synthesis conditions, especially the aggregation of surfactant by molecular recognition, plays an important role in controlling the size and shape of the final products. More detail regarding the nanostructure formation mechanism will be described in the following section.

Aside from TiO_2, other metal oxides in dendritic form also have been prepared in hydrothermal autoclaves. For example, in a cosolvent of ethanol and water, Zhang et al. prepared the dendritic structures of SnO_2 in rutile phase at 353 K by using stannous chloride as a precursor with added diammonium phosphate [62]. Based on the SEM images in Figure 3, it seemed that the product morphology was affected by the amount of phosphate. The authors claimed that (1) the pH value of the liquid phase was controlled by the amount of phosphate, which influenced the hydrolysis of stannous salt, and (2) different concentrations of phosphate could change the nucleation rates. Indeed, phosphate anions might form coordination transition metal cations [63], which would control the nucleation rate for the self-assembly process. A similar approach was used to synthesize many other dendritic oxides, such as cupric oxide [64], cuprous oxide [65], zinc oxide [66–69], cobalt oxide [70], cobalt doped nickel oxide [71], $CaTiO_3$ [72], $CuCo_2O_4$ [73], and $LaFeO_3$ [74].
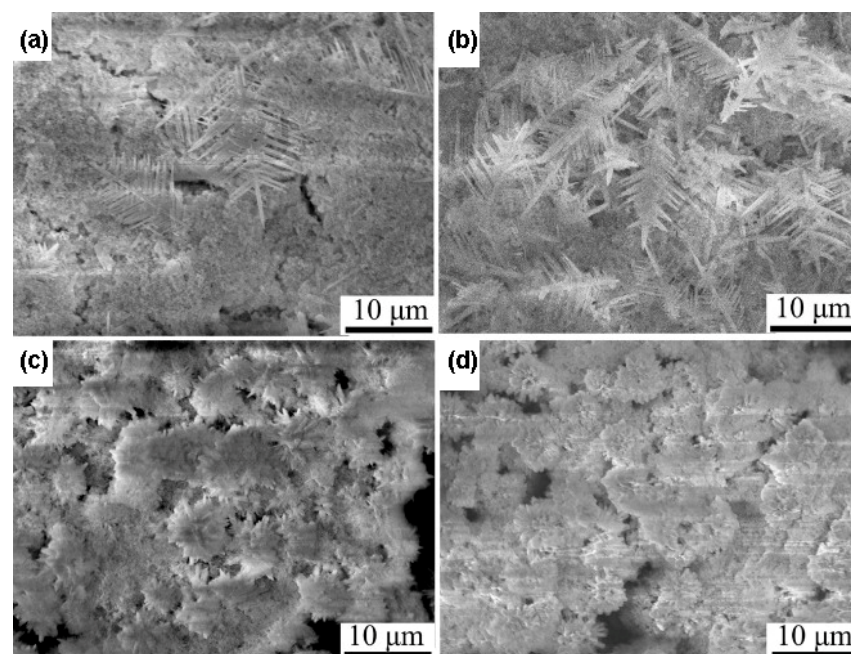

Figure 3. SEM images of SnO_2 leaf-like microstructure with different amounts of diammonium phosphate (**a**) 0.15 g, (**b**) 0.2 g, (**c**) 0.22 g, (**d**) 0.25 g. Reproduced from Ref. [62] with permission from Elsevier, 2018.

2.3. Electrochemical Synthesis

Surface roughness of materials is an important factor for friction, imbibition, wetting, and surface area [75,76]. To increase surface roughness of metal and oxides, one can use an electrochemical technique [77]. For example, Jeun and coworkers have demonstrated that a dendrite form of tin oxide can be prepared via an electrical deposition route. In their experiment, they selected electrolytes containing tin sulfate and sulfuric acid. The tin foam obtained was oxidized into dendritic tin oxide after annealing in air at 973 K, as revealed under electron microscope at different magnifications (Figure 4a,b) [78].
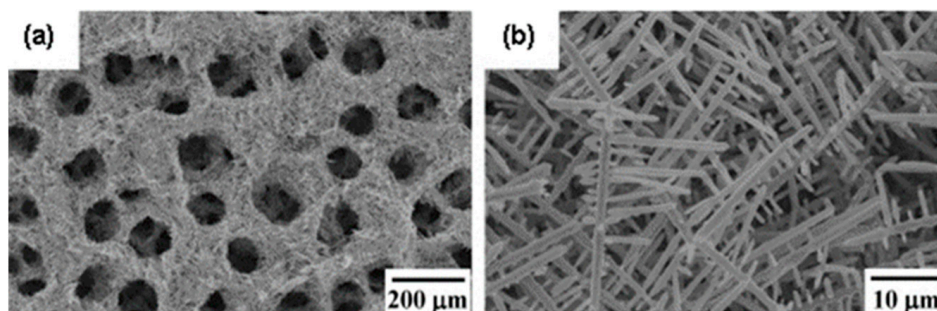

Figure 4. SEM images at two different magnifications (**a**) and (**b**) for Sn foams synthesized from electrochemically deposition after 15 s. Reproduced from Ref. [78] with permission from Elsevier, 2012.

2.4. Organic-Inorganic Hybrid materials

Nature has created remarkable organic-inorganic composite nanostructures, such as the materials found in diatom and mollusk shells in the past hundred million years of evolution on our planet. Humans have also learned a great deal on how to synthesize composite materials and have used them in a variety of applications such as Maya blue paint, dental fillers, and the structural materials for auto and aerospace industries [79]. To achieve desired chemical and physical properties, such as plasticity (from polymers) and mechanical strength (from inorganic fillers), self-assembly techniques are utilized to synthesize well-defined organic-inorganic composite materials [80,81]. For example, in-situ self-assembly can be carried out either by sol-gel reactions within polymer matrix or by polymerization of organic monomers from the surface of inorganic nanoparticles. Sometimes it is possible to simultaneously synthesize both organic and inorganic components [82–84].

One strategy for growing polymers from metal oxides is to modify the metal oxide surface with bifunctional molecules such as methacrylic acid, which has both carboxylic group and carbon double bonds. While carboxylic group can be anchored to TiO_2, the double bond can be used for the consequent in-situ polymerization of methyl methacrylate. As shown in Figure 5, poly(methyl methacrylate) (PMMA) can be pictured as branches on the titania domains [85]. The resulting materials provided improved dynamic Young's moduli with potential use as dental and bone fillers. Without chemical bond between the polymers and the TiO_2 fibers, the mechanical strength of the nanocomposite was found to be lower. This indicates that a dendritic polymer/inorganic nanocomposite has a better mechanical property than the counterpart made by a mechanical mixing of the organic and inorganic components. Besides the carboxylic functional group, phosphate groups can also be used to provide a chemical linkage between the organic and inorganic moieties [33,86,87]. Phosphorous dendrimers have been used to synthesize TiO_2 anatase crystals at a reaction temperature as low as 333 K without further calcination [75]. This approach may open a new avenue for one-pot or in-situ synthesis of organic-inorganic composite materials, as it avoids the normally required calcination procedure which can destroy the organic component.
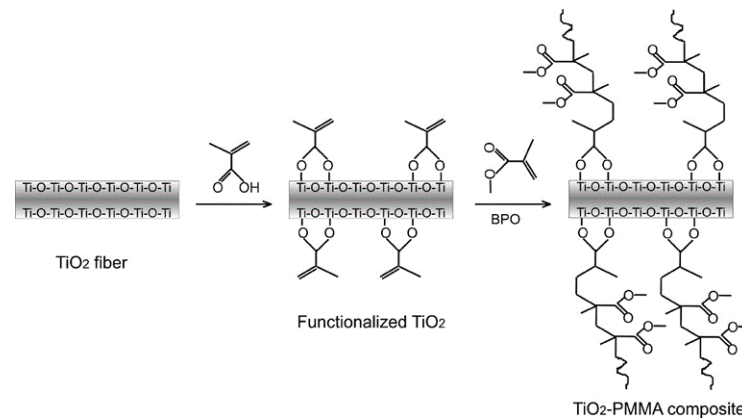
Figure 5. Schematic of functionalization of TiO$_2$ and formation of TiO$_2$-PMMA nanocomposite. Reproduced from Ref. [85] with permission from the ACS, 2007.

2.5. Supramolecular Dendrimers

Because supramolecular dendrimers with high quality and purity have potential for drug delivery, biosensor, and catalysis applications, many strategies have been explored for synthesizing these types of materials [88,89]. Here we selected an example of self-assembly of silsequioxane-based dendrimers, because the solvent's effect on the π-π stacking, hydrogen bonding, and van der Waals interactions were investigated [90]. In methyl methacrylate, π-π stacking of the dendrimer, as shown in Figure 6a, resulted in formation of linear supramolecules. These linear supramolecules formed bundles and thus can be observed with electron microscopes (Figure 6b,c,f,g). These bundles twisted together into secondary spherical structures with diameters >10 μm (see SEM images in Figure 6e), and finally, these secondary structures formed a solid network through gelation (Figure 6d). The resulting materials showed improved elasticity and viscosity.
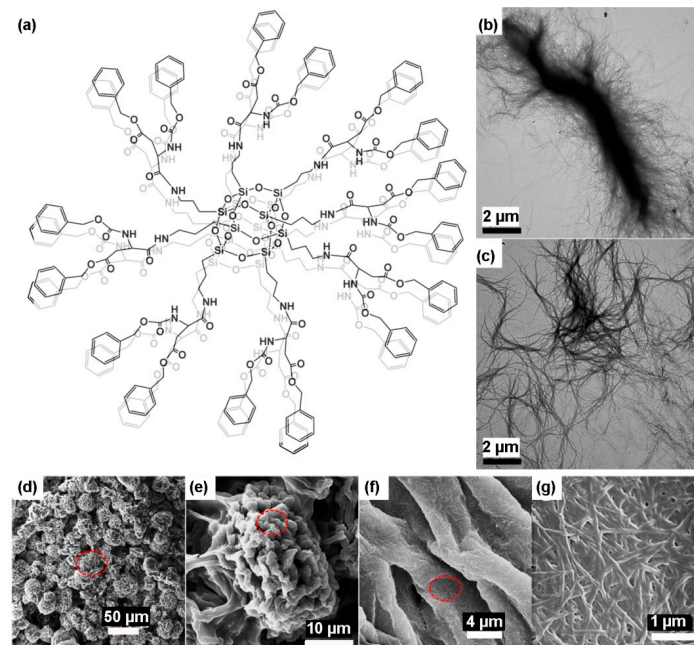

Figure 6. Chemical structure of a polyhedral oligomeric silsesquioxane core-based dendrimer (**a**). Stacking of this planar structure would form a linear structure which grows in the direction out of this paper. TEM (**b**,**c**) and SEM (**d**–**g**) images of the xerogel obtained in methyl methacrylate solvent under different magnifications. The red cycles highlight the areas where a higher magnification image was taken. Reproduced from Ref. [90] with permission from the ACS, 2017.

Interestingly, poly(propyleneimine) dendrimers have been used to synthesize encapsulated nanoparticles of metal and oxides [91]. By using the functional groups decorated within the dendrimers, such as amines, carboxylic acids, or hydroxyl groups, metal cations can be selectively trapped within the polymer matrix. After reduction of these cations, monodisperse nanoparticles can be obtained.

3. Dendritic Structure Formation Mechanism

3.1. Molecular Recognition for Dendritic Mesopore Formation

Micelles and reverse micelles have been widely used for making a variety of nanostructures. The driving forces for micelle formation can be from lyocratic, electrostatic or steric interactions [92]. To synthesize dendritic mesopores within silica, Yu and coworkers took advantage of a mixture of surfactants interacting with reactants: (cetyltrimethylammonium (CTA^+) tosylate), imidazolium ionic liquid (IL), triethanolamine ($TEAH_3$), triblock copolymer (F127), tetraethyl orthosilicate (TEOS), and water [93]. The aggregation of surfactant/ionic liquid micelles were believed to be responsible for the radially aligned mesopores (Figure 7). As a green solvent, the imidazolium IL behaved as a cosurfactant which reduced the critical micelle concentration of CTA^+. It was found that the silica size was affected by the alkyl chain length of IL, but the pore size within silica was not affected. Here the triblock copolymer was used to reduce the silica particle size. The silica with dendritic mesopores have potential in drug delivery, catalysis, and peptide separation [94].
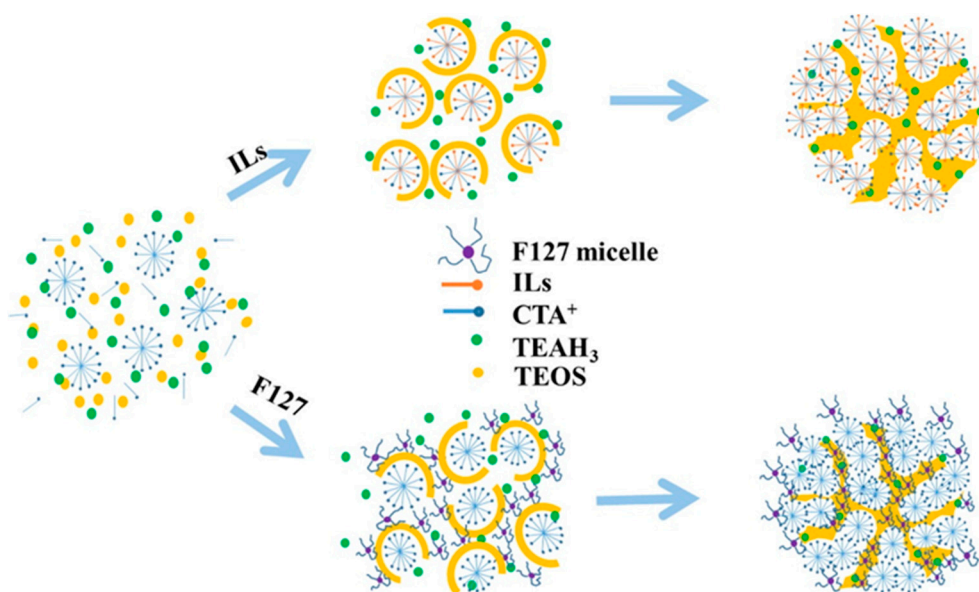

Figure 7. Mechanism for the synthesis of dendritic mesopores within silica nanoparticles with controllable particle size. Reproduced from Ref. [93] with permission from the ACS, 2014.

3.2. Sol-Gel Anisotropic-Assembly

As mentioned earlier, dendritic nanostructures of $Ti_6O_9(OAc)_6$ were produced by sol-gel reactions of titanium isopropoxide with acetic acid in supercritical CO_2 (Figure 2a,b). These structures arise due to the linear polycondensation of a reaction intermediate: $Ti_6O_6(OAc)_6(O^iPr)_6$ according to in-situ infrared and single crystal X-ray diffraction studies (Figure 8) [95,96]. The hexanuclear titanium cluster has six acetate bidentate around six titanium atoms, where the acetate groups do not undergo hydrolysis reaction. At the axial positions there are six isopropoxide that can be hydrolyzed. Condensation of these hydrolyzed complexes can lead to formation of linear oligomers and subsequent 1D nanostructures. These types of 1D structures were obtained in both supercritical CO_2 and heptanes under similar conditions [97]; however, dendritic structures were formed only in the supercritical condition. In heptanes, agglomeration of 1D structures resulted in a

3D porous network that filled the reactor. We hypothesized that, at the initial stage of the sol-gel process, the linear oligomers derived from $Ti_6O_6(OAc)_6(OH)_6$ need to have a high mobility to self-assembly into a branch structure. This is in line with the finding that both a higher diffusion and greater thermal motion of oligomers were important for controlling the self-assembly process [98–100]. A supercritical fluid is well-known to exhibit a low viscosity which facilitates both mass and heat transfer [101]; therefore, the dendritic structures should be more easily formed in supercritical CO_2 than in a traditional organic solvent. The leaf-like dendritic TiO_2 shown in Figure 2c,d was prepared in isopropanol. It was believed that the 2D structure was created through the self-assembly of a planar complex $(Ti_6O_4(O^iPr)_8(OAc)_8)$ [47]; however, it was not understood how the dendritic shape was produced. It seems that the core area of dendritic structure (Figure 2d) has totally different morphology compared to the leaves. Indeed, we have found some unidentified crystals under transmission electron microscope. It is hoped that these crystals would shed light on the mechanism of dendritic assembly.
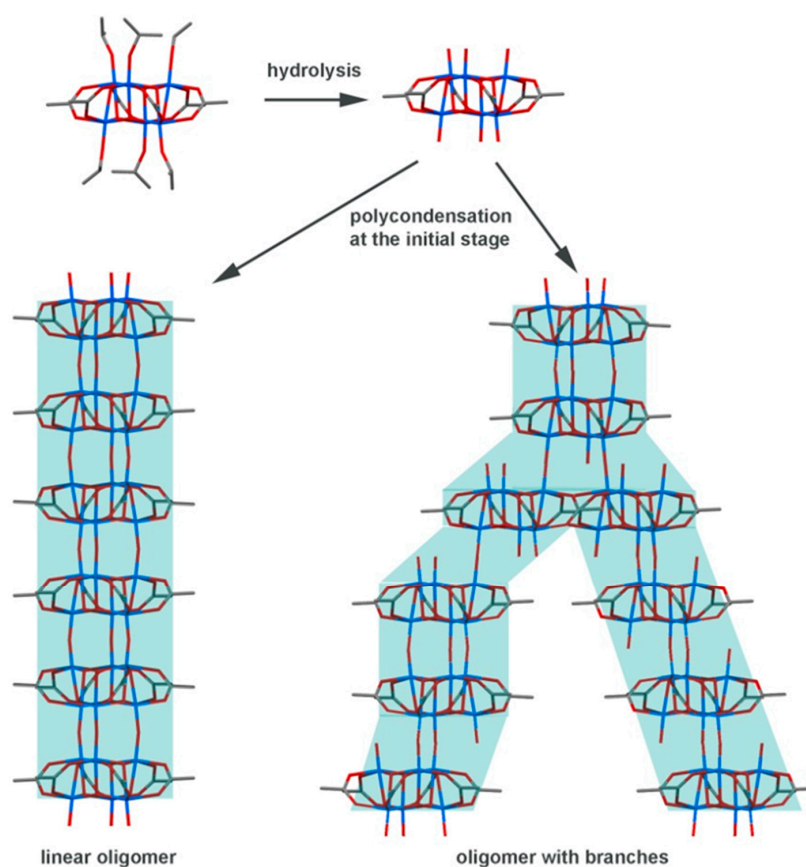

Figure 8. Hydrolysis and polycondensation of $Ti_6O_6(OAc)_6(O^iPr)_6$ can form linear or branched oligomers at the initial stage of sol-gel reactions. These oligomers may grow into agglomerated 1D and dendritic nanostructures in $scCO_2$. Note: Ti = blue; O = red; C = dark gray; H atoms omitted for clarity.

3.3. Hydrothermal Reactions

As described previously, hydrothermal and solvothermal reactions have been a popular approach for making dendritic metal oxides. Some ex-situ techniques, e.g., X-ray diffraction and electron microscopy, are helpful for nanostructure formation mechanism. In many cases, however, it is difficult to fully understand how the self-assembly process occurs. This is due to the challenge of limited in-situ techniques for a corrosive environment with elevated temperature and pressure.

Well-defined coniferous tree-like structures of iron oxide have been derived from hydrothermal reaction of potassium ferricyanide (Figure 9). In order to explain the mech-

anism of dendritic formation, Cao and colleagues carefully examined the orientation of the single crystals of hematite along the main stem and side branches [102]. It was found that the fast-growing main stem was along [1$\bar{1}$00] direction, while the side branches were along [10$\bar{1}$0] and [0$\bar{1}$10] directions. According to the authors, the crystallization kinetics are related to the surface net charge in each direction of a single crystal. A net neutral facet would facilitate a faster growth; on the other hand, a net charged facet would be affect more by solvent effect, which would decrease the growth in that direction. Interestingly, the magnetic property of the dendritic α-Fe$_2$O$_3$ was related where it is positioned in the dendritic structure. The morin transition temperature of the main stem was found higher (243 K) than that of branches (216 K). In a separate experiment, Wen and coworkers synthesized silver dendrites. They found that the main stem and branches grew along <100> and <111> directions, respectively. In addition, it seemed that the precursor molecule diffusions also played a role in the dendrite formation [103].
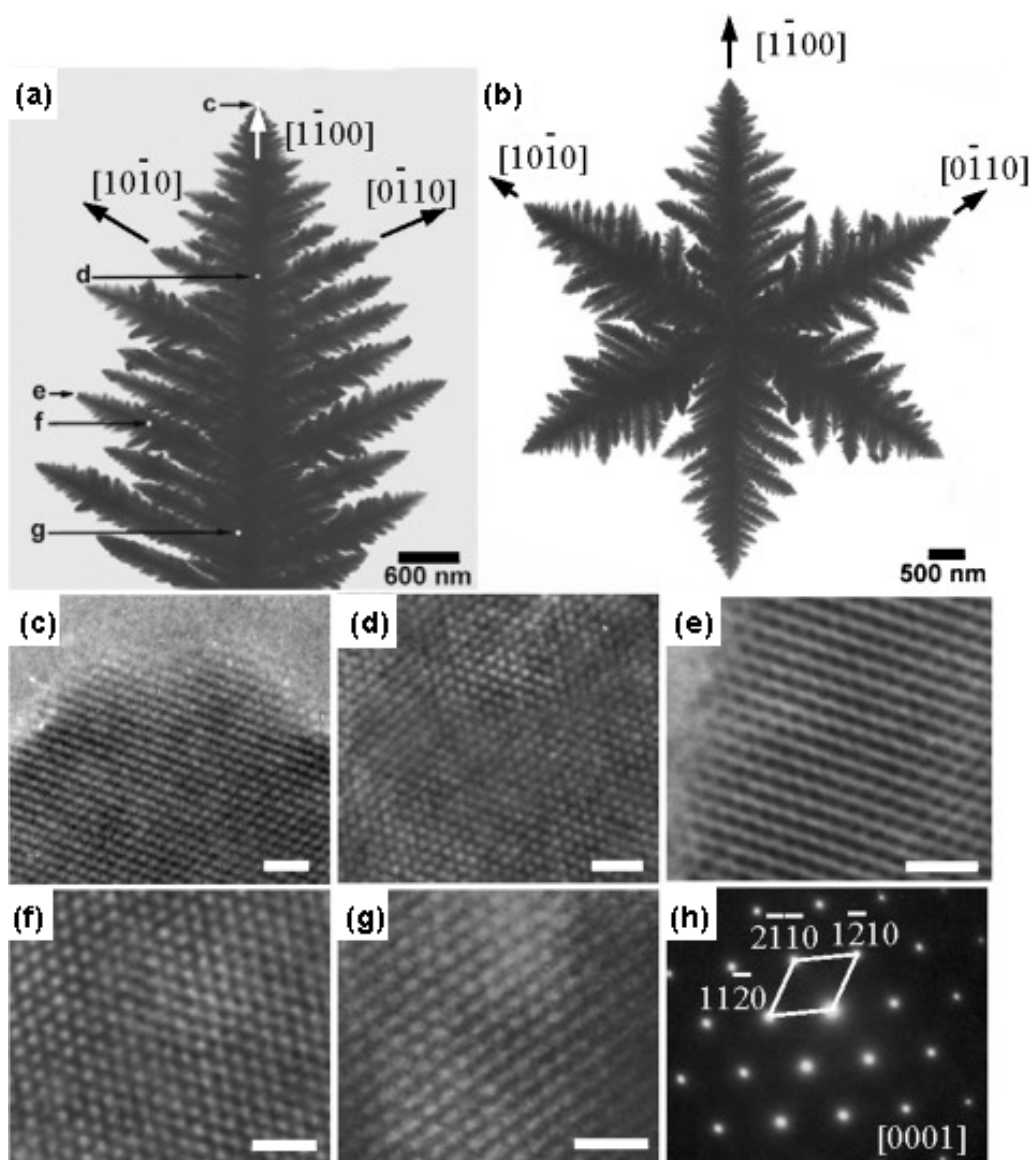

Figure 9. TEM of a fractal exhibiting hyperbranches of α-Fe$_2$O$_3$ fractals. (**b**) TEM image of a sixfold-symmetric dendritic structure. (**c–g**) High-resolution TEM images recorded in different regions of the dendritic structure in (**a**) showing the well-defined single-crystalline nature of the entire dendritic structure (scale bar: 1 nm). (**h**) Electron diffraction pattern recorded from the entire dendritic structure in (**a**) which also shows the single-crystalline nature of the entire dendritic structure. Reproduced from Ref. [102] with permission from Wiley-VCH, 2005.

During synthesis of dendritic rutile TiO_2, Sun and coworkers studied the surfactant's effect on the hydrothermal products. When cetyltrimethylammonium bromide (CTAB) was added to the titanium precursor with chloric acid, a dendritic structure composed of rods was produced. However, when ethylene glycol (EG) was added to the above mixture, the dendritic structure was made of nanoribbons versus rods. Furthermore, when both EG and urea were added to the mixture, the dendritic structures of nanofibers were produced (Figure 10) [104]. The authors proposed that ethylene glycol reduced the hydrolysis of the titanium precursor, and addition of urea impeded hydrolysis further, thus facilitating 2D and 1D nanostructure formation, respectively. The dendritic rutile TiO_2 was tested as anodes for lithium-ion batteries, which showed an enhanced charge capacity and extended life span. The authors attributed the better performance to the morphological advantages of dendritic TiO_2: (1) it facilitates the charge/discharge process of Li^+, and (2) a fast electron transfer along the 1D/2D TiO_2.
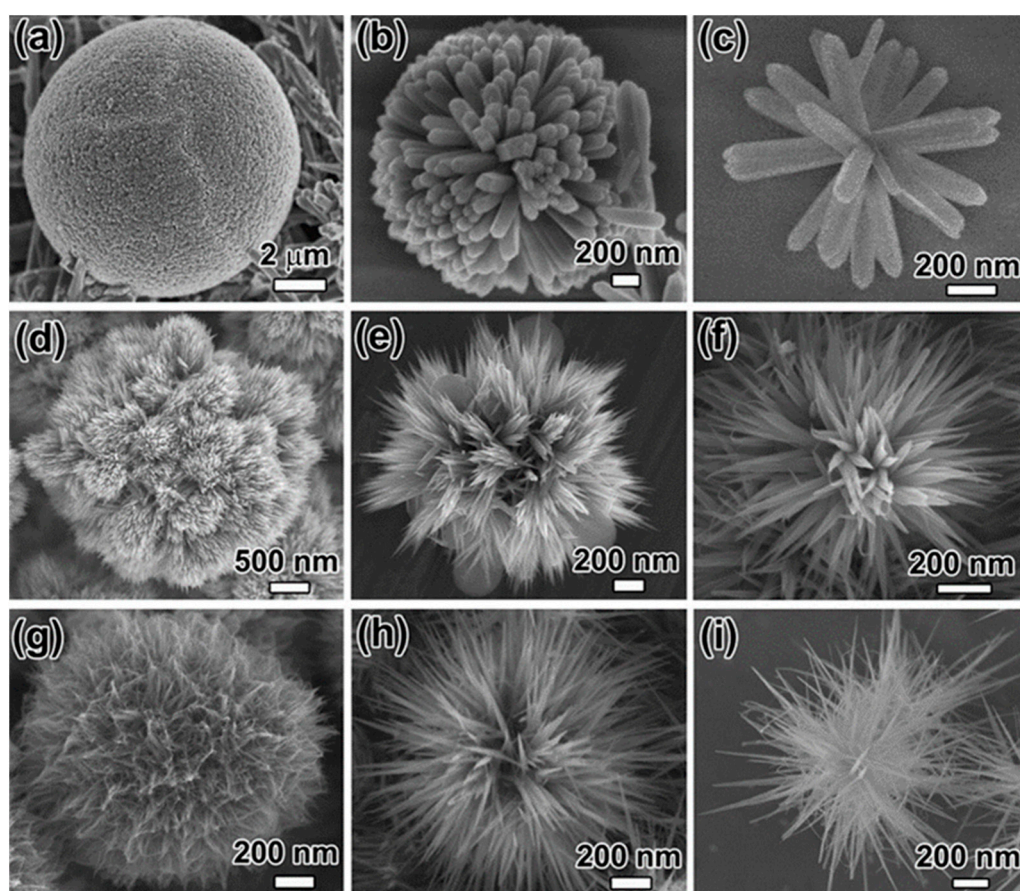

Figure 10. SEM images of 3D dendritic TiO_2 nanostructures: (**a–c**) 3D TiO_2 microspheres with nanorod building units obtained from aqueous titanium isopropoxide (TTIP) solutions having the composition of (**a**) $100H_2O$:7HCl:0.03CTAB:0.05TTIP, (**b**) $100H_2O$:7HCl:0.03CTAB:0.03TTIP, and (**c**) $100H_2O$:7HCl:0.03CTAB:0.01TTIP. (**d–f**) 3D TiO_2 microspheres with nanoribbon building units obtained from mixed solutions of aqueous TTIP solution ($100H_2O$:7HCl:0.03CTAB:0.05TTIP) and EG: (**d**) $TTIP_{aq}$:EG = 1:1, (**e**) $TTIP_{aq}$:EG = 1:2, and (**f**) $TTIP_{aq}$:EG = 1:3. (**g–i**) 3D TiO_2 microspheres with nanowire building units obtained from mixed solutions consisting of aqueous TTIP solution ($100H_2O$:7HCl:0.03CTAB:0.05TTIP) and EG, as well as 5 mmol of urea: (**g**) $TTIP_{aq}$:EG = 1:1, (**h**) $TTIP_{aq}$:EG = 1:2, and (**i**) $TTIP_{aq}$:EG = 1:3. Reproduced from Ref. [104] with permission from the ACS, 2011.

4. Applications

4.1. Conductometer Sensors

By using millions of olfactory receptor neurons and hundreds of functional genes, humans can distinguish thousands of odors. About 50% of people can recognize hydrogen sulfide (H_2S), a lethal gas, at a level as low as 4.7 ppb, which is more sensitive than many current H_2S monitors [105,106]. As shown in Figure 11, the olfactory receptor neurons contain dendrite structures, which collect odorant molecules in the back of the nasal cavity [107]. If the odorant molecules are recognized by the receptors, the latter will be activated and send an electric signal to the brain via nerve processes. Possibly inspired by the tree-like shape of olfactory receptors, many dendritic shaped biosensors have been investigated [108–110].
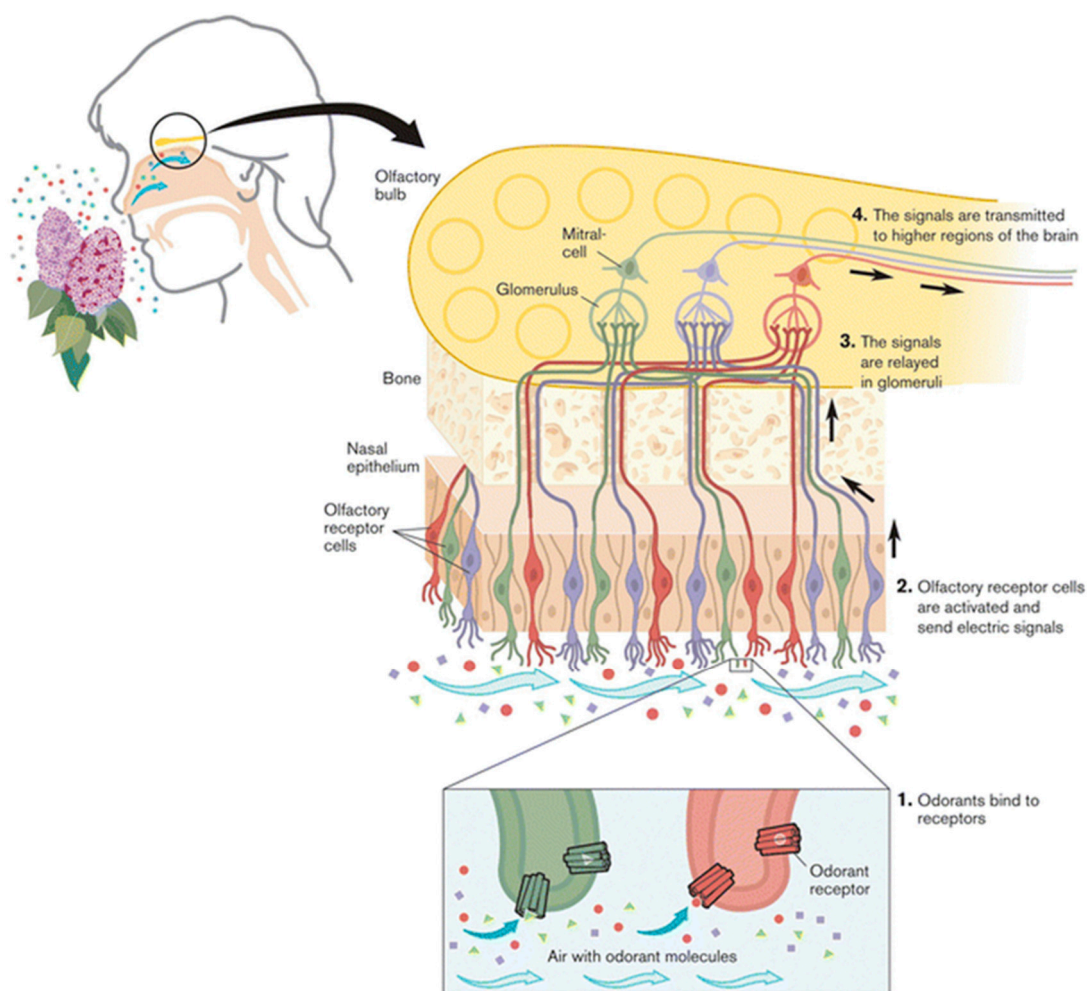

Figure 11. The human olfactory system. Reproduced from Ref. [107] with permission from Springer Nature, 2018.

Detective sensors are essential for warning and protecting people from exposure of poisonous gases. A thin film of metal oxide semiconductors can be used as the sensing material [111], because their conductivity changes after adsorption of certain gases. For example, n-type metal oxides (CuO, SnO_2, ZnO, and WO_3) are often used for conductometer sensors, because their higher carrier mobility than p-type metal oxides [112,113]. However, modified p-type metal oxides may also have a high sensitivity at a room temperature [114].

As an interesting example, p-type cuprous oxide (Cu_2O) was shown as an excellent sensing material for H_2S, because it generates Cu_xS on the surface after reacting with H_2S, and Cu_xS is known to have a high carrier mobility [115]. In addition, the detection sensitivity was significantly improved by taking advantage of accessible high

surface area of nanorods and dendritic Cu_2O, which were prepared by a sputtering process (Figures 12 and 13) [116]. This result is in line with the previous findings which indicate that semiconductor morphology is an important factor to determine the detector's sensibility [117]. The total surface electric resistance R_T can be estimated as below:

$$\frac{1}{R_T} = \frac{1}{R_S} + \frac{1}{R_B} + \frac{1}{R_{BR}} \tag{1}$$

where R_S, R_B, and R_{BR} are the resistive contributions of the surface, bulk, and dendritic structures, respectively. According to this equation, if R_{BR} decreases significantly upon exposure to H_2S, R_T would decrease accordingly.
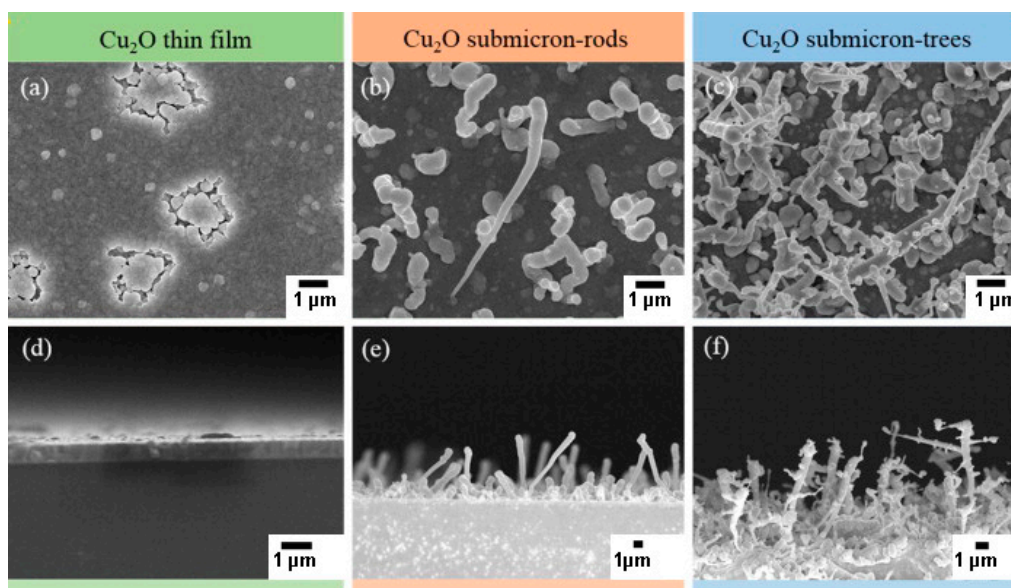
Figure 12. Top-view and cross-section FE-SEM images of Cu_2O thin film (**a**,**d**), submicron-rods (**b**,**e**) and submicron-trees (**c**,**f**). Reproduced from Ref. [116] with permission from Elsevier, 2014.
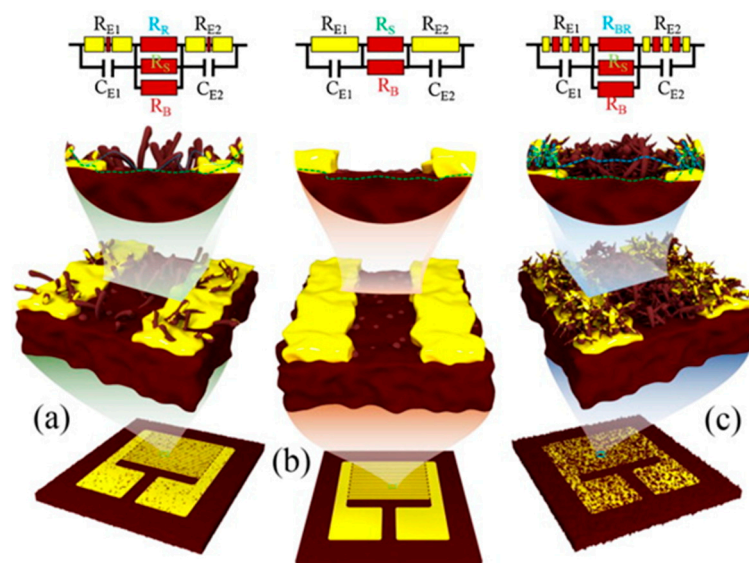
Figure 13. Models and equivalent circuit of the submicron-rod (**a**), thin film (**b**) and submicron-tree (**c**) sensors. It is noted that the total resistance will be reduced if R_R and R_{BR} decrease upon exposure to H_2S. Reproduced from Ref. [116] with permission from Elsevier, 2014.

It is worthy to mention that fluorescent dendrimers anchored on TiO_2 can be used as an optical sensor for detecting hazardous phenolic compounds [118].

4.2. Energy Conversion and Storages

Dendrimers, dendrites, and dendritic metal-oxides or sulfides are promising new materials for renewable energy, such as perovskite solar cells [119], water splitting [120], fuel cell [121], supercapacitors [122–125], as well as lithium-, sodium-, and zinc-ion batteries [126–129].

To reduce CO_2 emissions, the governments of many countries have recently been encouraged to invest and develop hydrogen as a fuel. Electrochemical water splitting can be a solution for producing hydrogen because water is abundant; however, the most effective electrode materials involve noble metals. To reduce the amount of noble metal required for making the electrodes, one can decorate platinum quantum dots on dendritic semiconductor nanostructures, or use highly efficient dendritic nanostructures of noble metal or oxide [130].

Electrochemical water splitting involves two half reactions: hydrogen evolution and oxygen evolution. To make an electrode for oxygen evolution reaction, Oh and coworkers deposited iridium dendrites on both carbon black and the hydrothermal synthesized antimony-doped tin oxide (Figure 14) [20]. The supported dendrites showed significantly higher electrocatalytic activity than the commercial iridium black. According to the authors, the increased catalytic performance of the dendrites was due to a larger surface area and more edge and corner atoms on the dendrite surface.
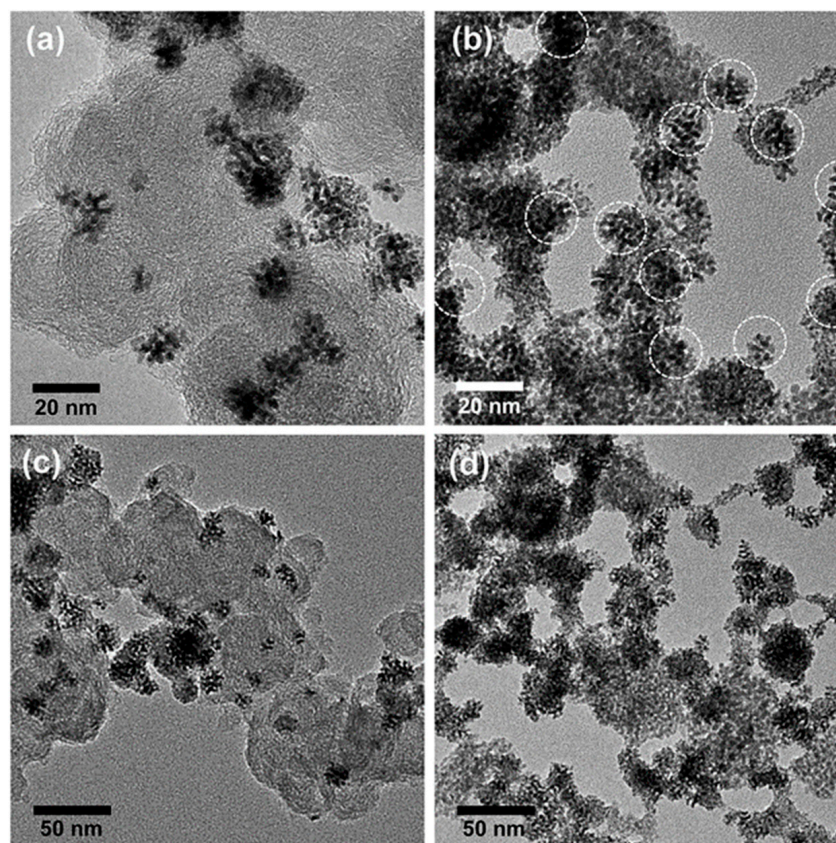

Figure 14. HR-TEM images of Ir-nanodendrite supported on (**a**) carbon black and (**b**) antimony-doped tin oxide. Low magnification TEM images of (**c**) Ir-nanodendrite/carbon and (**d**) Ir-nanodendrite/antimony-doped tin oxide. Reproduced from Ref. [20] with permission from the Royal Society of Chemistry, 2015.

4.3. Catalysis

Catalysts in dendritic form have been studied by many researchers [131–133]. After the excitement of exploring a new catalyst, it is essential to know if the dendritic form outperforms its counterparts in other morphologies, such as 0D, 1D, and 2D nanostructures. Based on specific surface area, all nanostructures are expected to have altered activity.

By comparing the effect of morphology on methanol electro-oxidation activity, Yin and coworkers found that palladium dendrites showed better performance than the corresponding nanoparticle format [134]. The authors argued that the void within the three-dimensional catalyst was the source of the activity difference between the two types of catalysts. Even though the pore size distributions were not available, the SEM images indeed showed that dendrites exhibited a larger void space (Figure 15). Larger pore size facilitates mass transfer, which is important for both reactant transport to the surface and product transport back to the bulk fluid. Hence, it is reasonable for the dendritic catalyst to outperform others. In another study, Au nanoparticles/TiO_2 and Au dendrites/TiO_2 were compared for their photocatalytic activity. There were no obvious specific catalytic differences between the two catalysts [135]. Nevertheless, it is noticed that the Au dendrites have a larger crystal size and thereby a smaller surface area than the particle counterpart. Therefore, Au dendrite should be more active than Au nanoparticles if the activity is on the basis of per active site or surface area of gold, i.e., if the turnover frequencies are considered equal.
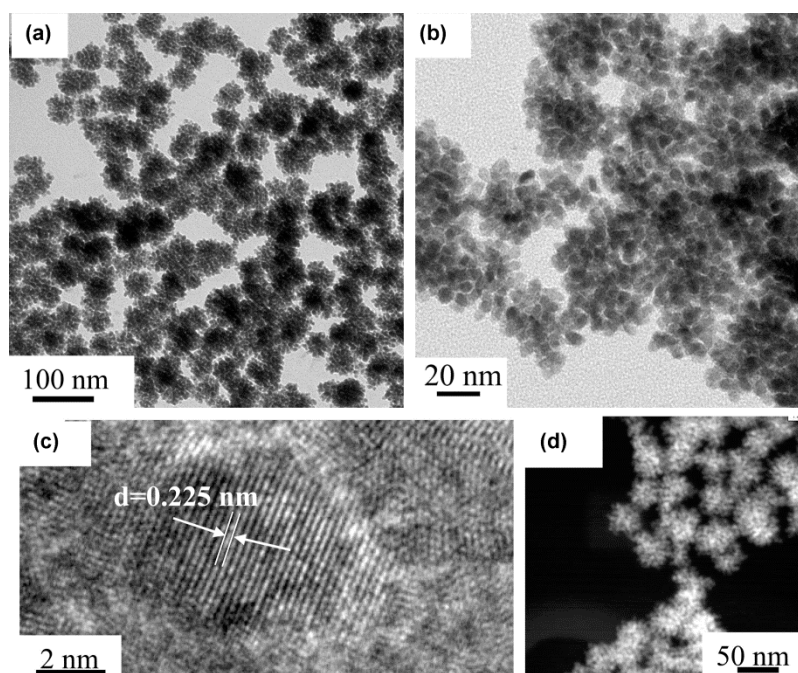
Figure 15. TEM images of Pd nanodendrites at different magnification (**a**,**b**); (**c**) HR-TEM image of Pd nanodendrites; (**d**) ADF-STEM image of Pd nanodendrites. Reproduced from Ref. [134] with permission from the ACS, 2009.

4.4. Drug Delivery

Dendritic metal oxides, especially modified SiO_2 with dendritic mesopores, have been extensively studied for their medical applications such as drug delivery [136] due to their biocompatibility, low toxicity, and tunable mesostructures.

Gai and coworkers incorporated iron oxide nanoparticles to control the morphology of SiO_2 that has dendritic pores, and used the resulting drug vehicles to deliver doxorubicin hydrochloride (DOX) into the nuclei of HeLa cells. The carboxylic groups of the drug molecules were able to form hydrogen bond with the surface OH-Si groups on SiO_2. Then, the drug was dissolved into phosphate buffer solution and diffused through the mesopore

channels of SiO_2. The in vitro studies showed a sustained drug release within 20 h, and the intracellular microscopic images revealed that the released DOX was active for killing tumor cells [137].

5. Conclusions

As an organized assembly of 1D or 2D nanostructures, dendritic metal oxide-related materials exhibit a high surface area/weight ratio and open large void space, which are important for their applications in sensing, catalysis, medicine, biomaterials, as well as energy conversion and storage devices. In designing electrode materials for lithium batteries and water splitting, for examples, attention should be paid to the morphological aspect of the semiconductive metal oxides besides the chemical compositions and crystalline phases. As described earlier, macrospores are essential for mass transfer within electrodes for water splitting process, but the mechanical strength of the materials may be reduced by introduce too many large pores. In addition, the orientation (e.g., the position of the pore openings) and the dimensions of the pore channels should make it easier for gas bubbles to escape in a liquid phase. Thus, the electrode materials must be carefully engineered. As another example, lithium-sulfur batteries have a high expectation for electrical cars because their high electrical storage capacity; however, the electrical capacity decreased too quickly after certain rounds of battery cycling. To solve this problem, one must increase the mobility of polysulfide ions. This can be achieved by increasing electrode pore size and promoting the polysulfide solubility. Another approach is to modify the electrode surface to increase the wettability of the sulfur cathode surface with sulfur and polysulfides [138]. Future work should be carried out in these fields by using carefully designed dendritic metal oxides.

While dendritic metal oxides have been synthesized via sol-gel or solvothermal techniques, molecular recognition is often responsible for the self-assembly process. Even though many dendritic nanostructures have already been made, their synthetic mechanism is still mainly elusive. Before we can truly design a controlled 3D structure, it is necessary to carry out more fundamental studies, including computational simulations, to provide a better understanding of both the underlying chemical reactions and self-assembly mechanisms.

Author Contributions: R.S.: conceptualization; original draft preparation. P.A.C.: formal analysis; review and editing; funding acquisition. R.A.M.: formal analysis; review and editing; funding acquisition. All authors have read and agreed to the published version of the manuscript.

Conflicts of Interest: The authors declare no conflict of interest. The sponsors had no role in the design, execution, interpretation, or writing of the study.

References

1. Seo, Y.; Manivannan, S.; Kang, I.; Lee, S.-W.; Kim, K. Gold dendrites Co-deposited with M13 virus as a biosensor platform for nitrite ions. *Biosens. Bioelectron.* **2017**, *94*, 87–93. [CrossRef] [PubMed]
2. Xie, X.-W.; Lv, J.-J.; Liu, L.; Wang, A.-J.; Feng, J.-J.; Xu, Q.-Q. Amino acid-assisted fabrication of uniform dendrite-like PtAu porous nanoclusters as highly efficient electrocatalyst for methanol oxidation and oxygen reduction reactions. *Int. J. Hydrog. Energ.* **2017**, *42*, 2104–2115. [CrossRef]
3. Buhleier, E.; Wehner, W.; Vögtle, F. "Cascade"- and "Nonskid-Chain-like" Syntheses of Molecular Cavity Topologies. *Synthesis* **1978**, *1978*, 155–158. [CrossRef]
4. Abbasi, E.; Aval, S.F.; Akbarzadeh, A.; Milani, M.; Nasrabadi, H.T.; Joo, S.W.; Hanifehpour, Y.; Nejati-Koshki, K.; Pashaei-Asl, R. Dendrimers: Synthesis, applications, and properties. *Nanoscale Res. Lett.* **2014**, *9*, 247. [CrossRef]
5. Ishiwari, F.; Shoji, Y.; Fukushima, T. Supramolecular scaffolds enabling the controlled assembly of functional molecular units. *Chem. Sci.* **2018**, *9*, 2028–2041. [CrossRef] [PubMed]
6. Roth, M.E.; Green, O.; Gnaim, S.; Shabat, D. Dendritic, Oligomeric, and Polymeric Self-Immolative Molecular Amplification. *Chem. Rev.* **2016**, *116*, 1309–1352. [CrossRef]
7. Wang, D.; Tong, G.; Dong, R.; Zhou, Y.; Shen, J.; Zhu, X. Self-assembly of supramolecularly engineered polymers and their biomedical applications. *Chem. Commun.* **2014**, *50*, 11994–12017. [CrossRef]

8. Ariga, K.; Nakanishi, T.; Hill, J.P. Self-assembled microstructures of functional molecules. *Curr. Opin. Colloid Interface Sci.* **2007**, *12*, 106–120. [CrossRef]

9. Astruc, D.; Chardac, F. Dendritic Catalysts and Dendrimers in Catalysis. *Chem. Rev.* **2001**, *101*, 2991–3024. [CrossRef]

10. Allabashi, R.; Arkas, M.; Hörmann, G.; Tsiourvas, D. Removal of some organic pollutants in water employing ceramic membranes impregnated with cross-linked silylated dendritic and cyclodextrin polymers. *Water Res.* **2007**, *41*, 476–486. [CrossRef]

11. Gasparotto, A.; Barreca, D.; Maccato, C.; Tondello, E. Manufacturing of inorganic nanomaterials: Concepts and perspectives. *Nanoscale* **2012**, *4*, 2813–2825. [CrossRef] [PubMed]

12. Tabacchi, G. Supramolecular Organization in Confined Nanospaces. *ChemPhysChem* **2018**, *19*, 1249–1297. [CrossRef]

13. Bekermann, D.; Barreca, D.; Gasparotto, A.; Maccato, C. Multi-component oxide nanosystems by Chemical Vapor Deposition and related routes: Challenges and perspectives. *CrystEngComm* **2012**, *14*, 6347–6358. [CrossRef]

14. Wei, H.; Xu, Q.; Li, A.; Wan, T.; Huang, Y.; Cui, D.; Pan, D.; Dong, B.; Wei, R.; Naik, N.; et al. Dendritic core-shell copper-nickel alloy@metal oxide for efficient non-enzymatic glucose detection. *Sens. Actuators B Chem.* **2021**, *337*, 129687. [CrossRef]

15. Darband, G.B.; Aliofkhazraei, M.; Shanmugam, S. Recent advances in methods and technologies for enhancing bubble detachment during electrochemical water splitting. *Renew. Sust. Energ. Rev* **2019**, *114*, 109300. [CrossRef]

16. Lei, Q.; Guo, J.; Noureddine, A.; Wang, A.; Wuttke, S.; Brinker, C.J.; Zhu, W. Sol–Gel-Based Advanced Porous Silica Materials for Biomedical Applications. *Adv. Funct. Mater.* **2020**, *30*, 1909539. [CrossRef]

17. González, B.; Ruiz-Hernández, E.; Feito, M.J.; López de Laorden, C.; Arcos, D.; Ramírez-Santillán, C.; Matesanz, C.; Portolés, M.T.; Vallet-Regí, M. Covalently bonded dendrimer-maghemite nanosystems: Nonviral vectors for in vitrogene magnetofection. *J. Mater. Chem.* **2011**, *21*, 4598–4604. [CrossRef]

18. Li, Z.; Yuan, D.; Jin, G.; Tan, B.H.; He, C. Facile Layer-by-Layer Self-Assembly toward Enantiomeric Poly(lactide) Stereocomplex Coated Magnetite Nanocarrier for Highly Tunable Drug Deliveries. *ACS Appl. Mater. Interface* **2016**, *8*, 1842–1853. [CrossRef]

19. Kundu, B.; Eltohamy, M.; Yadavalli, V.K.; Kundu, S.C.; Kim, H.-W. Biomimetic Designing of Functional Silk Nanotopography Using Self-assembly. *ACS Appl. Mater. Interface* **2016**, *8*, 28458–28467. [CrossRef] [PubMed]

20. Oh, H.-S.; Nong, H.N.; Reier, T.; Gliech, M.; Strasser, P. Oxide-supported Ir nanodendrites with high activity and durability for the oxygen evolution reaction in acid PEM water electrolyzers. *Chem. Sci.* **2015**, *6*, 3321–3328. [CrossRef]

21. Lamaka, S.V.; Shchukin, D.G.; Andreeva, D.V.; Zheludkevich, M.L.; Möhwald, H.; Ferreira, M.G.S. Sol-Gel/Polyelectrolyte Active Corrosion Protection System. *Adv. Funct. Mater.* **2008**, *18*, 3137–3147. [CrossRef]

22. Roussi, E.; Tsetsekou, A.; Tsiourvas, D.; Karantonis, A. Novel hybrid organo-silicate corrosion resistant coatings based on hyperbranched polymers. *Surf. Coat. Technol.* **2011**, *205*, 3235–3244. [CrossRef]

23. Tian, Z.; Shi, H.; Liu, F.; Xu, S.; Han, E.-H. Inhibiting effect of 8-hydroxyquinoline on the corrosion of silane-based sol–gel coatings on AA 2024-T3. *Prog. Org. Coat.* **2015**, *82*, 81–90. [CrossRef]

24. Wanka, R.; Koc, J.; Clarke, J.; Hunsucker, K.Z.; Swain, G.W.; Aldred, N.; Finlay, J.A.; Clare, A.S.; Rosenhahn, A. Sol–Gel-Based Hybrid Materials as Antifouling and Fouling-Release Coatings for Marine Applications. *ACS Appl. Mater. Interface* **2020**, *12*, 53286–53296. [CrossRef]

25. Angelos, S.; Johansson, E.; Stoddart, J.F.; Zink, J.I. Mesostructured Silica Supports for Functional Materials and Molecular Machines. *Adv. Funct. Mater.* **2007**, *17*, 2261–2271. [CrossRef]

26. Li, C.; Li, Q.; Kaneti, Y.V.; Hou, D.; Yamauchi, Y.; Mai, Y. Self-assembly of block copolymers towards mesoporous materials for energy storage and conversion systems. *Chem. Soc. Rev.* **2020**, *49*, 4681–4736. [CrossRef]

27. Li, Z.; Li, H.; Wu, Z.; Wang, M.; Luo, J.; Torun, H.; Hu, P.; Yang, C.; Grundmann, M.; Liu, X.; et al. Advances in designs and mechanisms of semiconducting metal oxide nanostructures for high-precision gas sensors operated at room temperature. *Mater. Horiz.* **2019**, *6*, 470–506. [CrossRef]

28. Huang, J.; Wan, Q. Gas Sensors Based on Semiconducting Metal Oxide One-Dimensional Nanostructures. *Sensors* **2009**, *9*, 9903–9924. [CrossRef] [PubMed]

29. Wasilewski, T.; Gębicki, J. Emerging strategies for enhancing detection of explosives by artificial olfaction. *Microchem. J.* **2021**, *164*, 106025. [CrossRef]

30. Yang, B.-X.; Tseng, C.-Y.; Chiang, A.S.-T.; Liu, C.-L. A sol–gel titanium–silicon oxide/organic hybrid dielectric for low-voltage organic thin film transistors. *J. Mater. Chem. C* **2015**, *3*, 968–972. [CrossRef]

31. Huang, H.; Liang, B.; Liu, Z.; Wang, X.; Chen, D.; Shen, G. Metal oxide nanowire transistors. *J. Mater. Chem.* **2012**, *22*, 13428–13445. [CrossRef]

32. Acton, O.; Ting Ii, G.G.; Ma, H.; Hutchins, D.; Wang, Y.; Purushothaman, B.; Anthony, J.E.; Jen, A.K.Y. π-σ-Phosphonic acid organic monolayer–amorphous sol–gel hafnium oxide hybrid dielectric for low-voltage organic transistors on plastic. *J. Mater. Chem.* **2009**, *19*, 7929–7936. [CrossRef]

33. Acton, B.O.; Ting, G.G.; Shamberger, P.J.; Ohuchi, F.S.; Ma, H.; Jen, A.K.Y. Dielectric Surface-Controlled Low-Voltage Organic Transistors via n-Alkyl Phosphonic Acid Self-Assembled Monolayers on High-k Metal Oxide. *ACS Appl. Mater. Interface* **2010**, *2*, 511–520. [CrossRef]

34. Hao, P.; Peng, B.; Shan, B.-Q.; Yang, T.-Q.; Zhang, K. Comprehensive understanding of the synthesis and formation mechanism of dendritic mesoporous silica nanospheres. *Nanoscale Adv.* **2020**, *2*, 1792–1810. [CrossRef]

35. Du, X.; Qiao, S.Z. Dendritic Silica Particles with Center-Radial Pore Channels: Promising Platforms for Catalysis and Biomedical Applications. *Small* **2015**, *11*, 392–413. [CrossRef] [PubMed]

36. Alfredsson, V.; Keung, M.; Monnier, A.; Stucky, G.D.; Unger, K.K.; Schüth, F. High-resolution transmission electron microscopy of mesoporous MCM-41 type materials. *J. Chem. Soc. Chem. Commun.* **1994**, *8*, 921–922. [CrossRef]

37. Dislich, H.; Hinz, P. History and principles of the sol-gel process, and some new multicomponent oxide coatings. *J. Non-Cryst. Solids* **1982**, *48*, 11–16. [CrossRef]

38. Uhlmann, D.R.; Teowee, G. Sol-Gel Science and Technology: Current State and Future Prospects. *J. Sol. Gel Sci. Technol.* **1998**, *13*, 153–162. [CrossRef]

39. Gesser, H.D.; Goswami, P.C. Aerogels and related porous materials. *Chem. Rev.* **1989**, *89*, 765–788. [CrossRef]

40. Hench, L.L.; West, J.K. The Sol-Gel Process. *Chem. Rev.* **1990**, *90*, 33–72. [CrossRef]

41. Sui, R.; Charpentier, P. Synthesis of metal oxide nanostructures by direct sol–gel chemistry in supercritical fluids. *Chem. Rev.* **2012**, *112*, 3057–3082. [CrossRef]

42. Brinker, C.J.; Scherer, G.W. *Sol-Gel Science: The Physics and Chemistry of Sol-Gel Processing*; Academic Press: New York, NY, USA, 1990.

43. Sanchez, C.; Livage, J.; Henry, M.; Babonneau, F. Chemical modification of alkoxide precursors. *J. Non-Cryst. Solids* **1988**, *100*, 65–76. [CrossRef]

44. Gash, A.E.; Tillotson, T.M.; Satcher, J.H.; Poco, J.F.; Hrubesh, L.W.; Simpson, R.L. Use of Epoxides in the Sol−Gel Synthesis of Porous Iron(III) Oxide Monoliths from Fe(III) Salts. *Chem. Mater.* **2001**, *13*, 999–1007. [CrossRef]

45. Benad, A.; Jürries, F.; Vetter, B.; Klemmed, B.; Hübner, R.; Leyens, C.; Eychmüller, A. Mechanical Properties of Metal Oxide Aerogels. *Chem. Mater.* **2018**, *30*, 145–152. [CrossRef]

46. Sui, R.; Rizkalla, A.S.; Charpentier, P.A. Formation of titania nanofibers: A direct sol-gel route in supercritical CO_2. *Langmuir* **2005**, *21*, 6150–6153. [CrossRef] [PubMed]

47. Sui, R.; Deering, C.E.; Prinsloo, R.; Lavery, C.B.; Chou, N.; Marriott, R.A. Sol–Gel Synthesis of 2-Dimensional TiO_2: Self-Assembly of Ti–Oxoalkoxy–Acetate Complexes by Carboxylate Ligand Directed Condensation. *Faraday Discuss.* **2021**, *227*, 125–140. [CrossRef]

48. Sui, R.; Lavery, C.B.; Li, D.; Deering, C.E.; Chou, N.; Dowling, N.I.; Marriott, R.A. Improving low-temperature CS_2 conversion for the Claus process by using La(III)-doped nanofibrous TiO_2 xerogel. *Appl. Catal. B* **2019**, *241*, 217–226. [CrossRef]

49. Lucky, R.A.; Charpentier, P.A. N-doped ZrO_2/TiO_2 bimetallic materials synthesized in supercritical CO_2: Morphology and photocatalytic activity. *Appl. Catal. B* **2010**, *96*, 516–523. [CrossRef]

50. Sui, R.; Lavery, C.B.; Deering, C.E.; Prinsloo, R.; Li, D.; Chou, N.; Lesage, K.L.; Marriott, R.A. Improved carbon disulfide conversion: Modification of an alumina Claus catalyst by deposition of transition metal oxides. *Appl. Catal. A Gen.* **2020**, *604*, 117773. [CrossRef]

51. Singh, S.; Singh, A.; Wan, M.; Yadav, R.R.; Tandon, P.; Rasool, S.S.A.; Yadav, B.C. Fabrication of self-assembled hierarchical flowerlike zinc stannate thin film and its application as liquefied petroleum gas sensor. *Sens. Actuators B Chem.* **2014**, *205*, 102–110. [CrossRef]

52. Souza, R.L.; Faria, E.L.P.; Figueiredo, R.T.; Fricks, A.T.; Zanin, G.M.; Santos, O.A.A.; Lima, Á.S.; Soares, C.M.F. Use of polyethylene glycol in the process of sol–gel encapsulation of Burkholderia cepacia lipase. *J. Therm. Anal. Calorim.* **2014**, *117*, 301–306. [CrossRef]

53. Islam, S.; Bidin, N.; Riaz, S.; Naseem, S. Self-assembled hierarchical phenolphthalein encapsulated silica nanoparticles: Structural, optical and sensing response. *Sens. Actuators A Phys.* **2017**, *266*, 111–121. [CrossRef]

54. Ibanez, A.; Maximov, S.; Guiu, A.; Chaillout, C.; Baldeck, P.L. Controlled Nanocrystallization of Organic Molecules in Sol-Gel Glasses. *Adv. Mater.* **1998**, *10*, 1540–1543. [CrossRef]

55. Gracheva, I.E.; Olchowik, G.; Gareev, K.G.; Moshnikov, V.A.; Kuznetsov, V.V.; Olchowik, J.M. Investigations of nanocomposite magnetic materials based on the oxides of iron, nickel, cobalt and silicon dioxide. *J. Phys. Chem. Solids* **2013**, *74*, 656–663. [CrossRef]

56. Sutar, P.; Suresh, V.M.; Jayaramulu, K.; Hazra, A.; Maji, T.K. Binder driven self-assembly of metal-organic cubes towards functional hydrogels. *Nat. Commun.* **2018**, *9*, 3587. [CrossRef]

57. Yoshimura, K.B.A.M. *Handbook of Hydrothermal Technology*; Cambridge University Press: Norwich, NY, USA, 2008.

58. Xiong, D.; Zhang, Q.; Du, Z.; Verma, S.K.; Li, H.; Zhao, X. Low temperature hydrothermal synthesis mechanism and thermal stability of p-type $CuMnO_2$ nanocrystals. *New J. Chem.* **2016**, *40*, 6498–6504. [CrossRef]

59. O'Hare, D. Hydrothermal Synthesis. In *Encyclopedia of Materials: Science and Technology*; Buschow, K.H.J., Cahn, R.W., Flemings, M.C., Ilschner, B., Kramer, E.J., Mahajan, S., Veyssière, P., Eds.; Elsevier: Oxford, UK, 2001; pp. 3989–3992.

60. Yin, H.; Wada, Y.; Kitamura, T.; Kambe, S.; Murasawa, S.; Mori, H.; Sakata, T.; Yanagida, S. Hydrothermal synthesis of nanosized anatase and rutile TiO_2 using amorphous phase TiO_2. *J. Mater. Chem.* **2001**, *11*, 1694–1703. [CrossRef]

61. Wu, Z.; Wu, Q.; Du, L.; Jiang, C.; Piao, L. Progress in the synthesis and applications of hierarchical flower-like TiO_2 nanostructures. *Particuology* **2014**, *15*, 61–70. [CrossRef]

62. Zhang, Y.; Li, D.; Qin, L.; Zhao, P.; Liu, F.; Chuai, X.; Sun, P.; Liang, X.; Gao, Y.; Sun, Y.; et al. Preparation and gas sensing properties of hierarchical leaf-like SnO_2 materials. *Sens. Actuators B Chem.* **2018**, *255*, 2944–2951. [CrossRef]

63. Murugavel, R.; Choudhury, A.; Walawalkar, M.G.; Pothiraja, R.; Rao, C.N.R. Metal Complexes of Organophosphate Esters and Open-Framework Metal Phosphates: Synthesis, Structure, Transformations, and Applications. *Chem. Rev.* **2008**, *108*, 3549–3655. [CrossRef]

64. Duan, Y.; Liu, X.; Han, L.; Asahina, S.; Xu, D.; Cao, Y.; Yao, Y.; Che, S. Optically Active Chiral CuO "Nanoflowers". *J. Am. Chem. Soc.* **2014**, *136*, 7193–7196. [CrossRef]

65. Janene, F.; Dhaouadi, H.; Etteyeb, N.; Touati, F. Flower-like cuprous oxide: Hydrothermal synthesis, optical, and electrochemical properties. *Ionics* **2015**, *21*, 477–485. [CrossRef]

66. Qiu, J.; Weng, B.; Zhao, L.; Chang, C.; Shi, Z.; Li, X.; Kim, H.-K.; Hwang, Y.-H. Synthesis and Characterization of Flower-Like Bundles of ZnO Nanosheets by a Surfactant-Free Hydrothermal Process. *J. Nanomater.* **2014**, *2014*, 281461. [CrossRef]

67. Kale, R.B.; Hsu, Y.-J.; Lin, Y.-F.; Lu, S.-Y. Hydrothermal synthesis, characterizations and photoluminescence study of single crystalline hexagonal ZnO nanorods with three dimensional flowerlike microstructures. *Superlattices Microstruct.* **2014**, *69*, 239–252. [CrossRef]

68. Jiang, C.; Zhang, W.; Zou, G.; Yu, W.; Qian, Y. Precursor-Induced Hydrothermal Synthesis of Flowerlike Cupped-End Microrod Bundles of ZnO. *J. Phys. Chem. B* **2005**, *109*, 1361–1363. [CrossRef]

69. Zhu, L.; Li, Y.; Zeng, W. Hydrothermal synthesis of hierarchical flower-like ZnO nanostructure and its enhanced ethanol gas-sensing properties. *Appl. Surf. Sci.* **2018**, *427*, 281–287. [CrossRef]

70. Yang, L.-X.; Zhu, Y.-J.; Li, L.; Zhang, L.; Tong, H.; Wang, W.-W.; Cheng, G.-F.; Zhu, J. A Facile Hydrothermal Route to Flower-Like Cobalt Hydroxide and Oxide. *Eur. J. Inorg. Chem.* **2006**, *2006*, 4787–4792. [CrossRef]

71. Xu, H.; Zeng, M.; Li, J.; Tong, X. Facile hydrothermal synthesis of flower-like Co-doped NiO hierarchical nanosheets as anode materials for lithium-ion batteries. *RSC Adv.* **2015**, *5*, 91493–91499. [CrossRef]

72. Dong, W.; Zhao, G.; Song, B.; Xu, G.; Zhou, J.; Han, G. Surfactant-free fabrication of $CaTiO_3$ butterfly-like dendrite via a simple one-step hydrothermal route. *CrystEngComm* **2012**, *14*, 6990–6997. [CrossRef]

73. Jadhav, H.S.; Pawar, S.M.; Jadhav, A.H.; Thorat, G.M.; Seo, J.G. Hierarchical Mesoporous 3D Flower-like CuCo2O4/NF for High-Performance Electrochemical Energy Storage. *Sci. Rep.* **2016**, *6*, 31120. [CrossRef] [PubMed]

74. Thirumalairajan, S.; Girija, K.; Ganesh, V.; Mangalaraj, D.; Viswanathan, C.; Ponpandian, N. Novel Synthesis of LaFeO3 Nanostructure Dendrites: A Systematic Investigation of Growth Mechanism, Properties, and Biosensing for Highly Selective Determination of Neurotransmitter Compounds. *Cryst. Growth Des.* **2013**, *13*, 291–302. [CrossRef]

75. Ensikat, H.J.D.-K.P.; Neinhuis, C.; Barthlott, W. Beilstein Superhydrophobicity in perfection: The outstanding properties of the lotus leaf. *J. Nanotechnol.* **2011**, *2*, 152–161.

76. Shin, S.; Seo, J.; Han, H.; Kang, S.; Kim, H.; Lee, T. Bio-Inspired Extreme Wetting Surfaces for Biomedical Applications. *Materials* **2016**, *9*, 116. [CrossRef] [PubMed]

77. Darmanin, T.; de Givenchy, E.T.; Amigoni, S.; Guittard, F. Superhydrophobic Surfaces by Electrochemical Processes. *Adv. Mater.* **2013**, *25*, 1378–1394. [CrossRef] [PubMed]

78. Jeun, J.-H.; Kim, D.-H.; Hong, S.-H. Synthesis of porous SnO_2 foams on SiO_2/Si substrate by electrochemical deposition and their gas sensing properties. *Sens. Actuators B Chem.* **2012**, *161*, 784–790. [CrossRef]

79. Sanchez, C.; Julián, B.; Belleville, P.; Popall, M. Applications of hybrid organic–inorganic nanocomposites. *J. Mater. Chem.* **2005**, *15*, 3559–3592. [CrossRef]

80. Cong, H.-P.; Yu, S.-H. Self-assembly of functionalized inorganic–organic hybrids. *Curr. Opin. Colloid Interface Sci.* **2009**, *14*, 71–80. [CrossRef]

81. Toksoz, S.; Acar, H.; Guler, M.O. Self-assembled one-dimensional soft nanostructures. *Soft Matter* **2010**, *6*, 5839–5849. [CrossRef]

82. Charpentier, P.A.; Li, X.; Sui, R. Study of the Sol-Gel Reaction Mechanism in Supercritical CO_2 for the Formation of SiO_2 Nanocomposites. *Langmuir* **2009**, *25*, 3748–3754. [CrossRef]

83. Zhao, S.; Malfait, W.J.; Jeong, E.; Fischer, B.; Zhang, Y.; Xu, H.; Angelica, E.; Risen, W.M.; Suggs, J.W.; Koebel, M.M. Facile One-Pot Synthesis of Mechanically Robust Biopolymer–Silica Nanocomposite Aerogel by Cogelation of Silicic Acid with Chitosan in Aqueous Media. *ACS Sustain. Chem. Eng.* **2016**, *4*, 5674–5683. [CrossRef]

84. Qu, L.; Hu, H.; Yu, J.; Yu, X.; Liu, J.; Xu, Y.; Zhang, Q. High-Yield Synthesis of Janus Dendritic Mesoporous Silica@Resorcinol–Formaldehyde Nanoparticles: A Competing Growth Mechanism. *Langmuir* **2017**, *33*, 5269–5274. [CrossRef] [PubMed]

85. Khaled, S.M.; Sui, R.; Charpentier, P.A.; Rizkalla, A.S. Synthesis of TiO2-PMMA nanocomposite: Using methacrylic acid as a coupling agent. *Langmuir* **2007**, *23*, 3988–3995. [CrossRef] [PubMed]

86. Katir, N.; Brahmi, Y.; Majoral, J.P.; Bousmina, M.; El Kadib, A. Ternary cooperative assembly—polymeric condensation of photoactive viologen, phosphonate-terminated dendrimers and crystalline anatase nanoparticles. *Chem. Commun.* **2015**, *51*, 17716–17719. [CrossRef] [PubMed]

87. Brahmi, Y.; Katir, N.; Hameau, A.; Essoumhi, A.; Essassi, E.M.; Caminade, A.-M.; Bousmina, M.; Majoral, J.-P.; El Kadib, A. Hierarchically porous nanostructures through phosphonate–metal alkoxide condensation and growth using functionalized dendrimeric building blocks. *Chem. Commun.* **2011**, *47*, 8626–8628. [CrossRef]

88. Fréchet, J.M.J. Dendrimers and supramolecular chemistry. *Proc. Natl. Acad. Sci. USA* **2002**, *99*, 4782. [CrossRef]

89. Lyu, Z.; Ding, L.; Tintaru, A.; Peng, L. Self-Assembling Supramolecular Dendrimers for Biomedical Applications: Lessons Learned from Poly(amidoamine) Dendrimers. *Acc. Chem. Res.* **2020**, *53*, 2936–2949. [CrossRef]

90. He, H.; Chen, S.; Tong, X.; An, Z.; Ma, M.; Wang, X.; Wang, X. Self-Assembly of a Strong Polyhedral Oligomeric Silsesquioxane Core-Based Aspartate Derivative Dendrimer Supramolecular Gelator in Different Polarity Solvents. *Langmuir* **2017**, *33*, 13332–13342. [CrossRef]

91. Scott, R.W.J.; Wilson, O.M.; Crooks, R.M. Synthesis, Characterization, and Applications of Dendrimer-Encapsulated Nanoparticles. *J. Phys. Chem. B* **2005**, *109*, 692–704. [CrossRef]

92. Fajalia, A.I.; Tsianou, M. Self-assembly control via molecular recognition: Effect of cyclodextrins on surfactant micelle structure and interactions determined by SANS. *Colloid. Surf. A Physicochem. Eng.* **2015**, *480*, 91–104. [CrossRef]

93. Yu, Y.-J.; Xing, J.-L.; Pang, J.-L.; Jiang, S.-H.; Lam, K.-F.; Yang, T.-Q.; Xue, Q.-S.; Zhang, K.; Wu, P. Facile Synthesis of Size Controllable Dendritic Mesoporous Silica Nanoparticles. *ACS Appl. Mater. Interface* **2014**, *6*, 22655–22665. [CrossRef]

94. Hong, Y.; Zhan, Q.; Zheng, Y.; Pu, C.; Zhao, H.; Lan, M. Hydrophilic phytic acid-functionalized magnetic dendritic mesoporous silica nanospheres with immobilized Ti^{4+}: A dual-purpose affinity material for highly efficient enrichment of glycopeptides/phosphopeptides. *Talanta* **2019**, *197*, 77–85. [CrossRef] [PubMed]

95. Sui, R.; Rizkalla, A.S.; Charpentier, P.A. FTIR study on the formation of TiO_2 nanostructures in supercritical CO_2. *J. Phys. Chem. B* **2006**, *110*, 16212–16218. [CrossRef]

96. Sui, R.; Thangadurai, V.; Berlinguette, C.P. Simple protocol for generating TiO_2 nanofibers in organic media. *Chem. Mater.* **2008**, *20*, 7022–7030. [CrossRef]

97. Sui, R.; Charpentier, P.A.; Marriott, R.A. Synthesizing 1D and 2D metal oxide nanostructures: Using metal acetate complexes as building blocks. *Nanoscale* **2020**, *12*, 17971–17981. [CrossRef]

98. Witten, T.A.; Sander, L.M. Diffusion-limited aggregation. *Phys. Rev. B* **1983**, *27*, 5686–5697. [CrossRef]

99. Abu-Much, R.; Meridor, U.; Frydman, A.; Gedanken, A. Formation of a Three-Dimensional Microstructure of Fe3O4−Poly(vinyl alcohol) Composite by Evaporating the Hydrosol under a Magnetic Field. *J. Phys. Chem. B* **2006**, *110*, 8194–8203. [CrossRef]

100. Wei-Hsiu, H.; Ming-Hao, H.; Shih-Shou, L. Enhanced photoluminescence of Alq3 via patterned array silver dendritic nanostructures. In Proceedings of the SPIE photonics Europe, Nanophotonics IV, Brussels, Belgium, 16–19 April 2012.

101. Johnston, K.P. New Directions in Supercritical Fluid Science and Technology. In *Supercritical Science and Technology*; Johnston, K.P., Penninger, J.M.L., Eds.; American Chemical Society: Washington, DC, USA, 1989; pp. 1–12.

102. Cao, M.; Liu, T.; Gao, S.; Sun, G.; Wu, X.; Hu, C.; Wang, Z.L. Single-Crystal Dendritic Micro-Pines of Magnetic α-Fe_2O_3: Large-Scale Synthesis, Formation Mechanism, and Properties. *Angew. Chem. Int. Ed.* **2005**, *44*, 4197–4201. [CrossRef] [PubMed]

103. Wen, X.; Xie, Y.-T.; Mak, W.C.; Cheung, K.Y.; Li, X.-Y.; Renneberg, R.; Yang, S. Dendritic Nanostructures of Silver: Facile Synthesis, Structural Characterizations, and Sensing Applications. *Langmuir* **2006**, *22*, 4836–4842. [CrossRef]

104. Sun, Z.; Kim, J.H.; Zhao, Y.; Bijarbooneh, F.; Malgras, V.; Lee, Y.; Kang, Y.-M.; Dou, S.X. Rational Design of 3D Dendritic TiO_2 Nanostructures with Favorable Architectures. *J. Am. Chem. Soc.* **2011**, *133*, 19314–19317. [CrossRef] [PubMed]

105. Sarafoleanu, C.; Mella, C.; Georgescu, M.; Perederco, C. The importance of the olfactory sense in the human behavior and evolution. *J. Med. Life* **2009**, *2*, 196–198. [PubMed]

106. Ropp, R.C. Chapter 3—Group 16 (O, S, Se, Te) Alkaline Earth Compounds. In *Encyclopedia of the Alkaline Earth Compounds*; Ropp, R.C., Ed.; Elsevier: Amsterdam, The Netherlands, 2013; pp. 105–197.

107. Carannante, I.; Marasco, A. Olfactory Sensory Neurons to Odor Stimuli: Mathematical Modeling of the Response. In *Encyclopedia of Computational Neuroscience*; Jaeger, D., Jung, R., Eds.; Springer: New York, NY, USA, 2018; pp. 1–12.

108. Sun, W.; Qi, X.; Zhang, Y.; Yang, H.; Gao, H.; Chen, Y.; Sun, Z. Electrochemical DNA biosensor for the detection of Listeria monocytogenes with dendritic nanogold and electrochemical reduced graphene modified carbon ionic liquid electrode. *Electrochim. Acta* **2012**, *85*, 145–151. [CrossRef]

109. Hashkavayi, A.B.; Raoof, J.B. Design an aptasensor based on structure-switching aptamer on dendritic gold nanostructures/ Fe_3O_4@SiO_2/DABCO modified screen printed electrode for highly selective detection of epirubicin. *Biosens. Bioelectron.* **2017**, *91*, 650–657. [CrossRef]

110. Hu, Y.; Zhang, Z.; Zhang, H.; Luo, L.; Yao, S. Selective and sensitive molecularly imprinted sol–gel film-based electrochemical sensor combining mercaptoacetic acid-modified PbS nanoparticles with Fe_3O_4@Au–multi-walled carbon nanotubes–chitosan. *J. Solid State Electrochem.* **2012**, *16*, 857–867. [CrossRef]

111. Firtat, B.; Moldovan, C.; Brasoveanu, C.; Muscalu, G.; Gartner, M.; Zaharescu, M.; Chesler, P.; Hornoiu, C.; Mihaiu, S.; Vladut, C.; et al. Miniaturised MOX based sensors for pollutant and explosive gases detection. *Sens. Actuators B Chem.* **2017**, *249*, 647–655. [CrossRef]

112. Mirzaei, A.; Kim, S.S.; Kim, H.W. Resistance-based H_2S gas sensors using metal oxide nanostructures: A review of recent advances. *J. Hazard. Mater.* **2018**, *357*, 314–331. [CrossRef] [PubMed]

113. Zhao, S.; Shen, Y.; Zhou, P.; Li, G.; Han, C.; Wei, D.; Zhong, X.; Zhang, Y.; Ao, Y. Influence of Synthesis Conditions on Microstructure and NO2 Sensing Properties of WO3 Porous Films Synthesized by Non-Hydrolytic Sol–Gel Method. *Nanomaterials* **2019**, *9*, 8. [CrossRef]

114. Dutt, M.; Ratan, A.; Tomar, M.; Gupta, V.; Singh, V. Mesoporous metal oxide–α-Fe_2O_3 nanocomposites for sensing formaldehyde and ethanol at room temperature. *J. Phys. Chem. Solids* **2020**, *145*, 109536. [CrossRef]

115. Lu, S.; Hu, W.; Hu, X. CuS_2 sheets: A hidden anode material with a high capacity for sodium-ion batteries. *J. Mater. Chem. C* **2021**, *9*, 1387–1395. [CrossRef]

116. Hien, V.X.; You, J.-L.; Jo, K.-M.; Kim, S.-Y.; Lee, J.-H.; Kim, J.-J.; Heo, Y.-W. H_2S-sensing properties of Cu_2O submicron-sized rods and trees synthesized by radio-frequency magnetron sputtering. *Sens. Actuators B Chem.* **2014**, *202*, 330–338. [CrossRef]

117. Comini, E. Metal oxides nanowires chemical/gas sensors: Recent advances. *Mater. Today Adv.* **2020**, *7*, 100099. [CrossRef]

118. Martínez-Ferrero, E.; Franc, G.; Mazères, S.; Turrin, C.-O.; Boissière, C.; Caminade, A.-M.; Majoral, J.-P.; Sanchez, C. Optical Properties of Hybrid Dendritic–Mesoporous Titania Nanocomposite Films. *Chem. Eur. J.* **2008**, *14*, 7658–7669. [CrossRef]

119. Pan, A.; Wu, Y.; Yan, K.; Yu, Y.; Jurow, M.J.; Ren, B.; Zhang, C.; Ding, S.; He, L.; Liu, Y. Stable Luminous Nanocomposites of Confined Mn^{2+}-Doped Lead Halide Perovskite Nanocrystals in Mesoporous Silica Nanospheres as Orange Fluorophores. *Inorg. Chem.* **2019**, *58*, 3950–3958. [CrossRef]

120. Zhang, P.; Li, L.; Nordlund, D.; Chen, H.; Fan, L.; Zhang, B.; Sheng, X.; Daniel, Q.; Sun, L. Dendritic core-shell nickel-iron-copper metal/metal oxide electrode for efficient electrocatalytic water oxidation. *Nat. Commun.* **2018**, *9*, 381. [CrossRef]

121. Delmondo, L.; Salvador, G.P.; Muñoz-Tabares, J.A.; Sacco, A.; Garino, N.; Castellino, M.; Gerosa, M.; Massaglia, G.; Chiodoni, A.; Quaglio, M. Nanostructured MnxOy for oxygen reduction reaction (ORR) catalysts. *Appl. Surf. Sci.* **2016**, *388*, 631–639. [CrossRef]

122. Maitra, S.; Mitra, R.; Nath, T.K. Investigation of electrochemical performance of $MgNiO_2$ prepared by sol-gel synthesis route for aqueous-based supercapacitor application. *Curr. Appl. Phys.* **2020**, *20*, 628–637. [CrossRef]

123. Mohd Abdah, M.A.A.; Azman, N.H.N.; Kulandaivalu, S.; Sulaiman, Y. Review of the use of transition-metal-oxide and conducting polymer-based fibres for high-performance supercapacitors. *Mater. Des.* **2020**, *186*, 108199. [CrossRef]

124. Zhang, H.; Ma, S.; Zhang, Q.; Cao, M.; Wang, Y.; Gu, Y.; Xu, X. Thermoreversible and Self-Protective Sol–Gel Transition Electrolytes for All-Printed Transferable Microsupercapacitors as Safer Micro-Energy Storage Devices. *ACS Appl. Mater. Interface* **2020**, *12*, 41819–41831. [CrossRef] [PubMed]

125. Patil, S.S.; Dubal, D.P.; Deonikar, V.G.; Tamboli, M.S.; Ambekar, J.D.; Gomez-Romero, P.; Kolekar, S.S.; Kale, B.B.; Patil, D.R. Fern-like $rGO/BiVO_4$ Hybrid Nanostructures for High-Energy Symmetric Supercapacitor. *ACS Appl. Mater. Interface* **2016**, *8*, 31602–31610. [CrossRef] [PubMed]

126. Yang, H.; Duh, J.-G. Aqueous sol–gel synthesized anatase TiO_2 nanoplates with high-rate capabilities for lithium-ion and sodium-ion batteries. *RSC Adv.* **2016**, *6*, 37160–37166. [CrossRef]

127. Wang, Z.; Guo, F.; Chen, C.; Shi, L.; Yuan, S.; Sun, L.; Zhu, J. Self-Assembly of PEI/SiO_2 on Polyethylene Separators for Li-Ion Batteries with Enhanced Rate Capability. *ACS Appl. Mater. Interface* **2015**, *7*, 3314–3322. [CrossRef]

128. Duan, M.; Meng, Y.; Zhang, H.; Zhao, G.; Hu, J.; Ren, G.; Zhu, F. Facile synthesis of graphene-like carbon-coated Ni_3S_2 nanoparticles self-assembled on 3D dendritic nanostructure as high-performance anode materials of sodium-ion batteries. *Ionics* **2020**, *26*, 4511–4522. [CrossRef]

129. Wei, T.; Li, Q.; Yang, G.; Wang, C. High-rate and durable aqueous zinc ion battery using dendritic $V10O_{24} \cdot 12H_2O$ cathode material with large interlamellar spacing. *Electrochim. Acta* **2018**, *287*, 60–67. [CrossRef]

130. Ye, B.; Huang, L.; Hou, Y.; Jiang, R.; Sun, L.; Yu, Z.; Zhang, B.; Huang, Y.; Zhang, Y. Pt (111) quantum dot decorated flower-like αFe_2O_3 thin film nanosheets as a highly efficient bifunctional electrocatalyst for overall water splitting. *J. Mater. Chem. A* **2019**, *7*, 11379–11386. [CrossRef]

131. Du, X.; Zhao, C.; Luan, Y.; Zhang, C.; Jaroniec, M.; Huang, H.; Zhang, X.; Qiao, S.-Z. Dendritic porous yolk@ordered mesoporous shell structured heterogeneous nanocatalysts with enhanced stability. *J. Mater. Chem. A* **2017**, *5*, 21560–21569. [CrossRef]

132. Xue, X.-L.; Lang, W.-Z.; Yan, X.; Guo, Y.-J. Dispersed Vanadium in Three-Dimensional Dendritic Mesoporous Silica Nanospheres: Active and Stable Catalysts for the Oxidative Dehydrogenation of Propane in the Presence of CO_2. *ACS Appl. Mater. Interface* **2017**, *9*, 15408–15423. [CrossRef]

133. Beshkar, F.; Amiri, O.; Salavati-Niasari, M.; Beshkar, F. Novel dendrite-like $CuCr_2O_4$ photocatalyst prepared by a simple route in order to remove of Azo Dye in textile and dyeing wastewater. *J. Mater. Sci. Mater. Electron.* **2015**, *26*, 8182–8192. [CrossRef]

134. Yin, Z.; Zheng, H.; Ma, D.; Bao, X. Porous Palladium Nanoflowers that Have Enhanced Methanol Electro-Oxidation Activity. *J. Phys. Chem. C* **2009**, *113*, 1001–1005. [CrossRef]

135. Bannat, I.; Wessels, K.; Oekermann, T.; Rathousky, J.; Bahnemann, D.; Wark, M. Improving the Photocatalytic Performance of Mesoporous Titania Films by Modification with Gold Nanostructures. *Chem. Mater.* **2009**, *21*, 1645–1653. [CrossRef]

136. Maity, A.; Polshettiwar, V. Dendritic Fibrous Nanosilica for Catalysis, Energy Harvesting, Carbon Dioxide Mitigation, Drug Delivery, and Sensing. *ChemSusChem* **2017**, *10*, 3866–3913. [CrossRef]

137. Gai, S.; Yang, P.; Ma, P.A.; Wang, D.; Li, C.; Li, X.; Niu, N.; Lin, J. Fibrous-structured magnetic and mesoporous Fe_3O_4/silica microspheres: Synthesis and intracellular doxorubicin delivery. *J. Mater. Chem.* **2011**, *21*, 16420–16426. [CrossRef]

138. Fotouhi, A.; Auger, D.J.; Propp, K.; Longo, S.; Wild, M. A review on electric vehicle battery modelling: From Lithium-ion toward Lithium–Sulphur. *Renew. Sustain. Energy Rev.* **2016**, *56*, 1008–1021. [CrossRef]